Article

Cell

Cell-Type-Specific Alternative Splicing Governs Cell Fate in the Developing Cerebral Cortex

Graphical Abstract

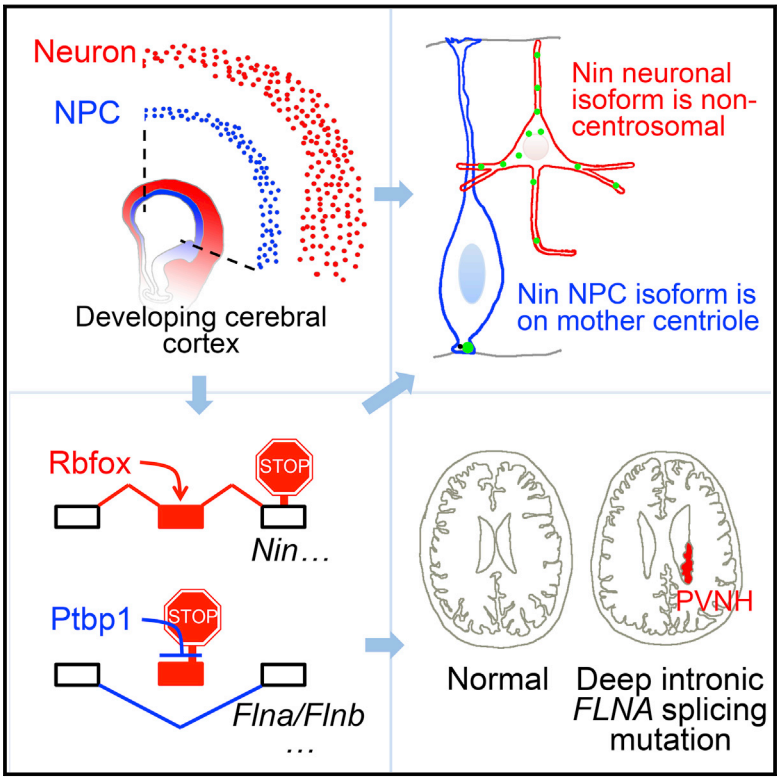

Authors

Xiaochang Zhang, Ming Hui Chen, Xuebing Wu, ..., Peter V. Kharchenko, Phillip A. Sharp, Christopher A. Walsh

Correspondence

xiaochang.zhang@childrens.harvard.edu (X.Z.), christopher.walsh@childrens.harvard.edu (C.A.W.)

In Brief

Moving beyond observation of widespread alternative splicing in the brain, regulated changes in alternative splicing patterns between neural progenitors and neurons are shown to drive cortical development in mice and humans.

Highlights

- Alternative exons distinguish progenitors and neurons in developing cerebral cortex
- Rbfox-mediated alternative splicing removes Ninein from centrosome for neurogenesis
- An intronic mutation de-represses a *FLNA* poison exon, leading to brain malformation
- Ptbp1 and Rbfox antagonistically regulate neuronal exon inclusion and neuronal fate

Data Resources

GSE76198

Zhang et al., 2016, Cell *166*, 1147–1162
August 25, 2016
http://dx.doi.org/10.1016/j.cell.2016.07.025

CellPress

Cell

Cell-Type-Specific Alternative Splicing Governs Cell Fate in the Developing Cerebral Cortex

Xiaochang Zhang,[1,2,*] Ming Hui Chen,[1,3] Xuebing Wu,[4,5] Andrew Kodani,[6] Jean Fan,[7,8] Ryan Doan,[1,2] Manabu Ozawa,[9] Jacqueline Ma,[1] Nobuaki Yoshida,[9] Jeremy F. Reiter,[6] Douglas L. Black,[10] Peter V. Kharchenko,[7,8] Phillip A. Sharp,[4] and Christopher A. Walsh[1,2,8,11,12,*]

[1]Division of Genetics and Genomics, Manton Center for Orphan Disease Research, Howard Hughes Medical Institute, Boston Children's Hospital, Boston, MA 02115, USA

[2]Departments of Neurology and Pediatrics, Harvard Medical School, Boston, MA 02115, USA

[3]Department of Cardiology, Boston Children's Hospital and Harvard Medical School, Boston, MA 02215, USA

[4]David H. Koch Institute for Integrative Cancer Research, Department of Biology, Computational and Systems Biology Graduate Program, Massachusetts Institute of Technology, Cambridge, MA 02139, USA

[5]Whitehead Institute for Biomedical Research, Cambridge, MA 02142, USA

[6]Department of Biochemistry and Biophysics, Cardiovascular Research Institute, University of California, San Francisco, San Francisco, CA 94158, USA

[7]Department of Biomedical Informatics, Harvard Medical School, Boston, MA 02115, USA

[8]Harvard Stem Cell Institute, Cambridge, MA 02138, USA

[9]Laboratory of Developmental Genetics, Center for Experimental Medicine and Systems Biology, The University of Tokyo, Tokyo 108-8639, Japan

[10]Department of Microbiology, Immunology, and Molecular Genetics, University of California, Los Angeles, Los Angeles, CA 90095, USA

[11]Broad Institute of MIT and Harvard, Cambridge, MA 02142, USA

[12]Lead Contact

*Correspondence: xiaochang.zhang@childrens.harvard.edu (X.Z.), christopher.walsh@childrens.harvard.edu (C.A.W.)

http://dx.doi.org/10.1016/j.cell.2016.07.025

SUMMARY

Alternative splicing is prevalent in the mammalian brain. To interrogate the functional role of alternative splicing in neural development, we analyzed purified neural progenitor cells (NPCs) and neurons from developing cerebral cortices, revealing hundreds of differentially spliced exons that preferentially alter key protein domains—especially in cytoskeletal proteins—and can harbor disease-causing mutations. We show that Ptbp1 and Rbfox proteins antagonistically govern the NPC-to-neuron transition by regulating neuron-specific exons. Whereas Ptbp1 maintains apical progenitors partly through suppressing a poison exon of *Flna* in NPCs, Rbfox proteins promote neuronal differentiation by switching Ninein from a centrosomal splice form in NPCs to a non-centrosomal isoform in neurons. We further uncover an intronic human mutation within a PTBP1-binding site that disrupts normal skipping of the *FLNA* poison exon in NPCs and causes a brain-specific malformation. Our study indicates that dynamic control of alternative splicing governs cell fate in cerebral cortical development.

INTRODUCTION

The neocortex is phylogenetically the newest part of the human brain, with its projection neurons originating from waves of neurogenesis initiated by apical radial glial (aRG) cells, followed by extensive radial neuronal migration (Gao et al., 2014; Greig et al., 2013; Huttner et al., 2013; Lui et al., 2011). Radial glial cells (RGCs) maintain long basal processes attached to the pial membrane and undergo mitosis near their apical processes in the ventricular zone (VZ) or outer subventricular zone (oSVZ) to self-renew or produce other types of progenitors, including intermediate progenitors (IPs). IPs undergo limited numbers of divisions to produce neurons. In humans, the massive expansion of the cortex is accompanied by additional numbers of cell divisions, progenitor types, and neuronal circuits by mechanisms that are poorly understood (Lui et al., 2011).

Alternative splicing (AS) regulates over 90% of multi-exon protein-coding genes in humans and exerts an evolutionarily conserved posttranscriptional control on genome-wide and tissue-specific gene expression (Barbosa-Morais et al., 2012; Merkin et al., 2012; Wang et al., 2008). Transcriptional profiling of mammalian forebrain has revealed dynamic AS changes between different brain regions (Johnson et al., 2009), cortical layers (Belgard et al., 2011), or developmental stages (Dillman et al., 2013; Yan et al., 2015). Dysregulation of AS in human brain by *RBFOX1* mutations or disturbed nSR100 levels has been associated with intellectual disability and autism spectrum disorders (ASDs) (Bhalla et al., 2004; Irimia et al., 2014; Sebat et al., 2007). nSR100, Ptbp1, and Rbfox proteins have also been reported to regulate AS of neuronal microexons (Irimia et al., 2014; Li et al., 2015). Recent studies have generated an unprecedented view of AS in cortical development (Darnell, 2013; Li et al., 2007; Raj and Blencowe, 2015; Vuong et al., 2016), but the physiological impact of AS on cortical progenitor and neuronal fates remains unclear. On the one hand, systematic studies of cortical neural progenitor cells (NPCs) concentrated mostly on gene-level instead of exon-level expression or

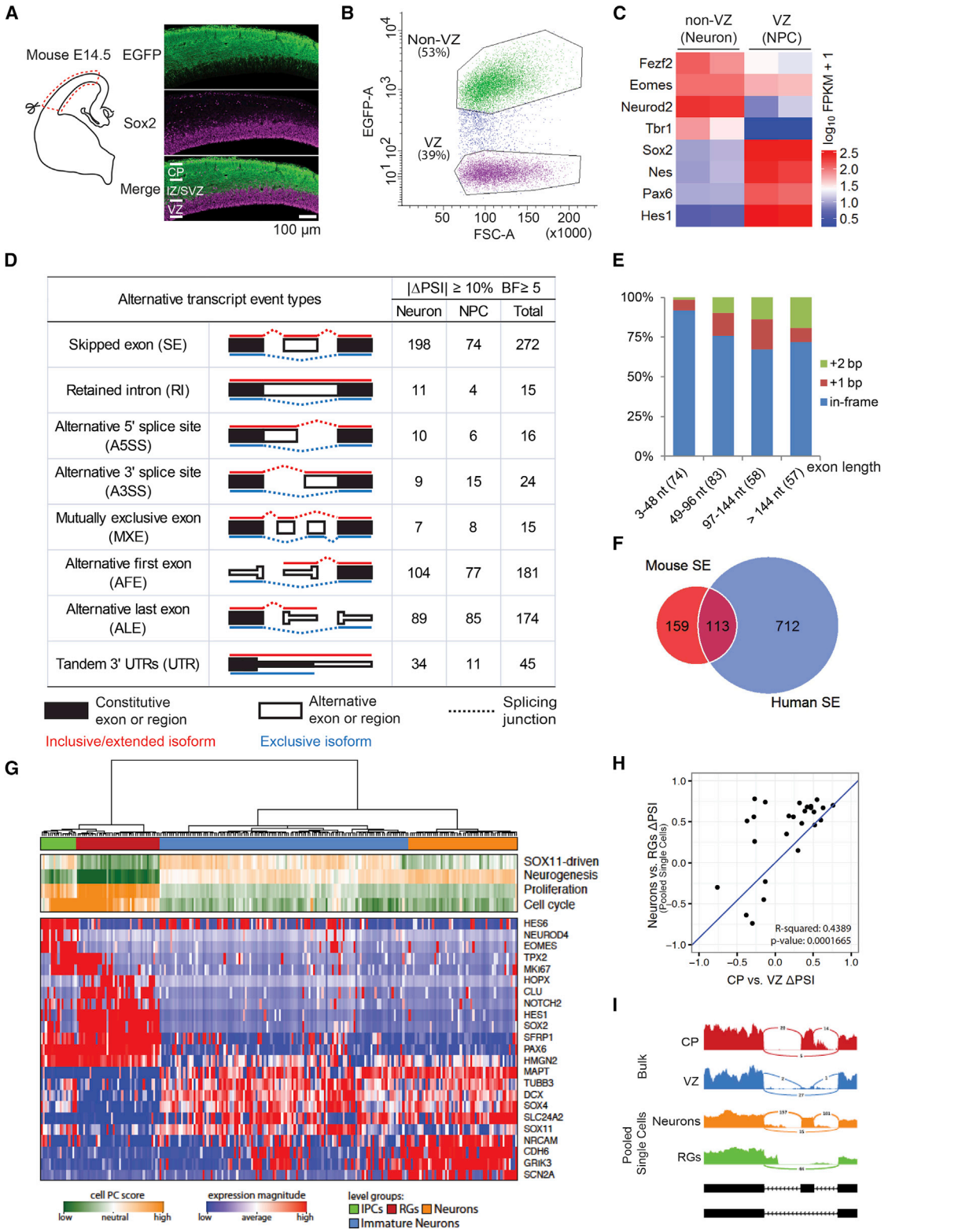

Figure 1. Extensive and Conserved Alternative Exon Usages during Cerebral Cortical NPC Differentiation

(A) Immunostaining of E14.5 *Tbr2-EGFP* mouse dorsal cerebral cortex with anti-EGFP (green) and anti-Sox2 (magenta).

(B) Fluorescence-activated cell sorting (FACS) of green and non-green cells from E14.5 *Tbr2-EGFP* mouse dorsal cerebral cortex.

(legend continued on next page)

detected rather subtle AS changes (Ayoub et al., 2011). On the other hand, previous AS studies of the developing cerebral cortex centered on either RNA-binding proteins (RBPs) or individual alternative exons, rather than taking a global view of cell-type-specific regulation. Direct comparative investigations of alternative exon usage between cortical NPCs and neurons in a physiological context are not yet available.

We performed unbiased RNA sequencing (RNA-seq) comparison of NPCs and neurons isolated directly from developing mouse and human cerebral cortices and identified extensive and conserved AS switches during cortical NPC differentiation. We found that AS preferentially regulates genes encoding cytoskeleton proteins, modulates protein subcellular localization, and involves genes essential for brain development in mice and/or humans. Our results on dynamic switching of Ninein and filamin A isoforms by Rbfox1/2/3 and Ptbp1 proteins reveal developmental roles of AS in regulating centriolar dynamics, NPC self-renewal, and differentiation, uncovering widespread functions of AS in cerebral cortical development.

RESULTS

RNA-Seq of Sorted NPCs and Neurons from Developing Mouse Cerebral Cortex Uncovers Extensive Alternative Exon Usage during Cortical NPC Differentiation

Using a *Tbr2-EGFP* transgene driving EGFP in dorsal cortex (Figure S1A; Gong et al., 2003), we found that embryonic day 14.5 (E14.5) VZ NPCs (Sox2+; EGFP−) are well separated from IPs in the subventricular zone (SVZ) (Tbr2+; EGFP+) and differentiating neurons in the intermediate zone (IZ) and cortical plate (CP) (Sox2−; EGFP+; Figures 1A and S1A). We isolated VZ NPCs (EGFP−) and non-VZ cells (EGFP+) from E14.5 *Tbr2-EGFP* cerebral cortex (Figure 1B) and confirmed their identities: (1) strand-specific RNA-seq and qPCR of sorted cells showed that NPC genes *Sox2*, *Pax6*, *Nes*, and *Hes1* were highly enriched in the (EGFP−) cells whereas *Tbr1*, *Fezf2*, and *Neurod2* were enriched in the (EGFP+) cells (Figures 1C and S1B); (2) the fourth exon of REST, expressed in differentiating neurons (Raj et al., 2011), was depleted from sorted (EGFP−) cells (Figure S1C); (3) 93.5% of sorted (EGFP−) cells were Sox2 positive (Figures S1D and S1E); and (4) gene ontology analysis revealed that cell cycle, chromosomal, and DNA metabolic genes were enriched in (EGFP−) cells, whereas neuron differentiation and projection genes were enriched in (EGFP+) cells (Figure S1F). These results indicate that we successfully isolated and analyzed VZ NPCs (EGFP−) and a mixture of differentiating neurons outside the VZ (hereafter referred to as non-VZ or neuron) from developing mouse cerebral cortex.

We compared alternative exon usage between E14.5 VZ NPCs and non-VZ cells using the mixture-of-isoforms (MISO) statistical model, which assigned a "percentage spliced in" (PSI) value to each exon by estimating its abundance compared to adjacent exons (Katz et al., 2010). We found that 622 exons were differentially spliced between mouse NPCs and neurons ($|\Delta PSI| \geq 10\%$ and Bayes factor ≥ 5; the same criteria used hereafter if not specified), with 345 showing higher inclusion in neurons and 277 higher in NPCs. We analyzed VZ and CP samples from two additional RNA-seq datasets (Ayoub et al., 2011; Fietz et al., 2012) and found 742 AS changes shared by at least two of the three datasets (Figures 1D and S1G). Two hundred seventy-two cassette exons or skipped exons (SE) comprised the largest portion of AS events, with 198 (73%) SEs showing higher inclusion in neurons than in NPCs (Figure 1D), 255 (94%) SEs shorter than 300 nt (Figure S1H), and 61 (22%) SEs causing frameshifts (Figure 1E). These results indicate that hundreds of alternative exon usages occur when VZ NPCs differentiate in mice.

Extensive Alternative Exon Usage during NPC Differentiation in the Developing Human Cerebral Cortex

The developing human cortex has an enormously expanded oSVZ housing the largest population of dividing progenitors, the most prominent being outer radial glial (oRG) cells that resemble aRG cells but lack apical processes. We compared laser microdissected oSVZ to VZ, inner SVZ (iSVZ), and CP (Fietz et al., 2012), as well as RNA-seq data from purified aRG and oRG cells (Johnson et al., 2015), and found that most splicing switches occur between neural progenitors in the VZ and neurons in the CP (2,582 exons; Figures S1I and S1J), with 31% of human cassette exons ($|\Delta PSI| \geq 15\%$; Bayes factor ≥ 10) causing a translational frameshift (Figure S1K). When SE, A3SS, A5SS, mutually exclusive exons (MXE), and retained introns (RI) (Figure 1D) were considered, 38% of mouse differential splicing events were also differentially spliced in human, including 113/272 (42%) mouse SEs (Figure 1F).

To compare AS between pure NPC and neuronal populations, we further analyzed RNA-seq data of 224 single cells from three human fetal cortices (Camp et al., 2015). Using the unbiased pathway and gene set overdispersion analysis approach (PAGODA) (Fan et al., 2016), we were able to identify distinct transcriptional subpopulations corresponding to RGs, IPs, immature neurons, and neurons (Figure 1G). We then pooled single RGs and single neurons in silico and extended our MISO analysis to these putatively pure RG and mature neuron populations, which gave rise to 298 significant cassette exon changes.

(C) Heatmap of RNA-seq results showing differential gene expression between sorted VZ and non-VZ cells.
(D) Number of alternative exons between neural progenitor cells (NPCs) and differentiating neurons.
(E) Histogram showing the size of mouse SEs (x axis) and the percentages of SEs that cause an in-frame insertion or a frameshift (y axis).
(F) Conserved SEs in mouse and human cortical neurogenesis.
(G) PAGODA analysis distinguishes 224 single fetal cortical cells (Camp et al., 2015) into four clusters (green, blue, red, and yellow). Shown at the bottom are gene expression patterns for selected marker genes.
(H) ΔPSI scores between pooled single cells and bulk samples show significant correlation.
(I) Sashimi plots from bulk and single-cell analyses showing the last three exons of *CERS5*.
See also Figure S1.

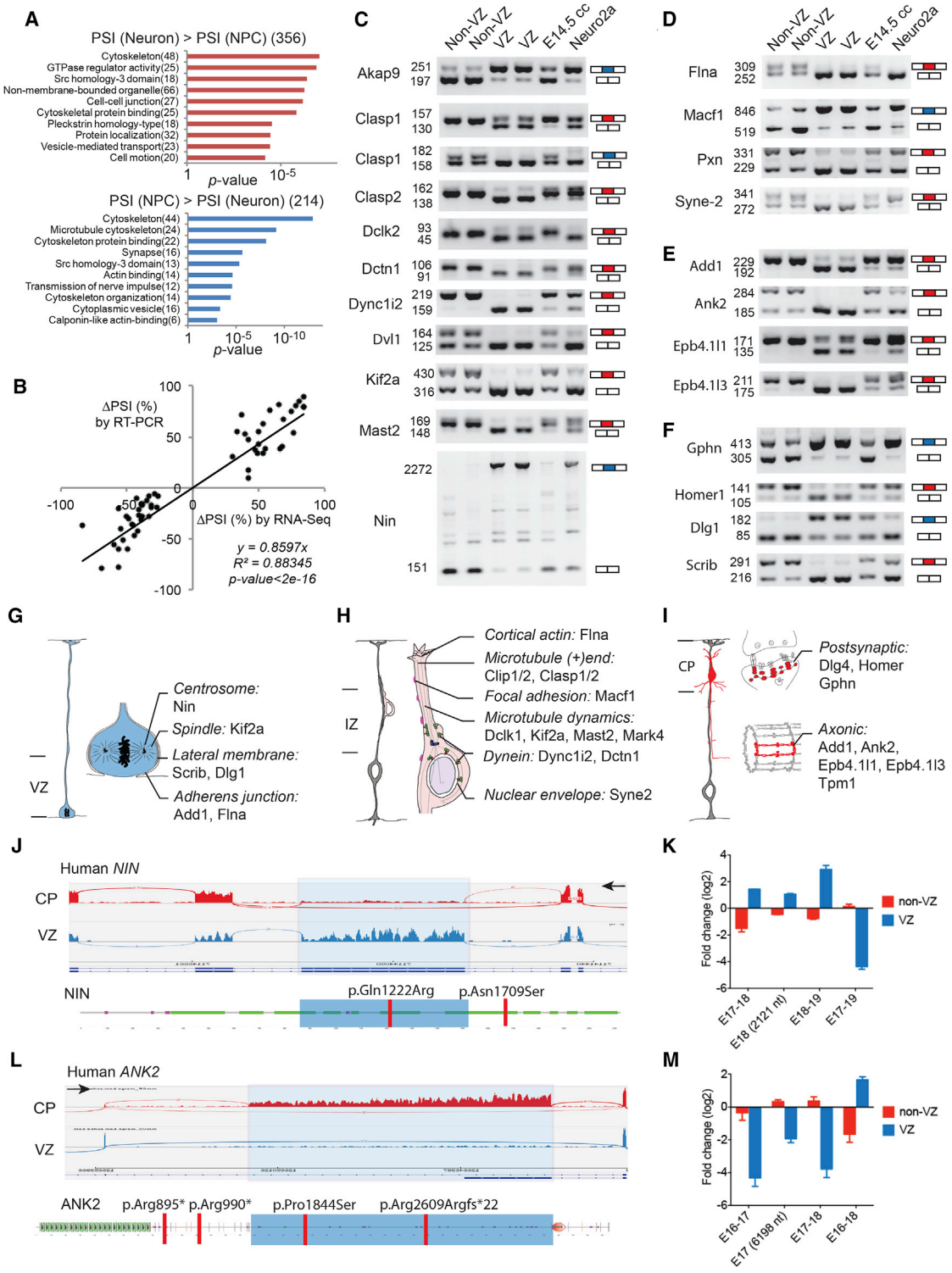

Figure 2. Alternative Splicing Preferentially Regulates Genes Encoding Cytoskeleton Proteins

(A) Ontology analysis of genes that are alternatively spliced between E14.5 mouse NPCs and differentiating neurons, showing the top ten ranked terms and count of genes (in parentheses).

(B) RT-PCR analyses validate 57 AS events identified by MISO. ΔPSI = PSI (neuron) – PSI (NPC).

(C–F) RT-PCR validation of alternatively spliced SEs related to microtubule (C), actin (D), Add1-Ank2-Epb4.1 complex (E), and synapse (F). "E14.5 cc" represents unsorted E14.5 mouse cerebral cortex.

(legend continued on next page)

Consistent with bulk samples, more SEs show higher inclusion in neurons (166) than in RGs (132). For 26 SEs that were also identified in human bulk samples, ΔPSIs are significantly correlated between bulk and pooled single-cell analyses (p value = 1.7e−4; Figures 1H and 1I). These results indicate that extensive alternative exon usages occur when VZ NPCs differentiate in mouse and human cerebral cortex and many of them may critically regulate gene function by shifting translational frames, though we focus here mainly on those shared by mouse and human to allow functional analysis of their mechanism.

Cytoskeleton Genes Are Preferentially Regulated by Alternative Splicing during Neurogenesis

Gene ontology analysis for differentially spliced exons revealed that cytoskeleton genes are overrepresented in mouse and human (Figures 2A, S2A, and S2B). Kyoto Encyclopedia of Genes and Genomes (KEGG) pathway analyses of alternative exons also revealed enriched functions in regulating tight junctions and actin cytoskeleton (Figure S2C; data not shown). Differential mouse SEs between E14.5 NPCs and neurons were validated by RT-PCR, and many of these events were switch-like (|ΔPSI| > 50%; Figures 2B–2F, S2D, and S2E; Table S1). Notably, alternatively spliced cytoskeleton genes encoded functionally interconnected protein networks (Figures 2G–2I) involved in NPC proliferation, neuronal migration, and neuronal differentiation. Over a dozen genes alternatively spliced during the NPC-to-neuron transition—including *Add1*, *Ank2*, *Flna*, *Kif2a*, *Macf1*, *Scrib*, and *Syne2*—have previously been shown to be required for normal cerebral cortical development in mice (Table S2), and certain alternative exons harbor mutations that associate with human brain disorders, such as microcephaly and autism (Figures 2J–2M and below), suggesting cell-type-specific mechanisms of human diseases.

Alternatively Spliced Exons Alter Protein Domains and Subcellular Localization

Exons that are differentially spliced between NPCs and neurons are remarkable in the extent to which they critically involve essential protein domains. Among 61 splicing changes in 49 genes regulating cytoskeleton (Table S3), 20 (33%) of them caused insertion or deletion of one or more entire protein domains (Figures 3A, 3B, and S3A–S3C). Multiple genes showed AS of membrane-targeting domains (Figure 3B), which typically regulate subcellular localization. Another 13 (21%) alternative exons—including a microexon—inserted extra amino acids (extraAAs) into well-defined protein domains (Figures 3A, S3A, and S3C). Thus, more than half (54%) of differentially spliced regions directly regulate protein domains.

Alternative Splicing Switches Ninein from Centrosome in NPCs to Non-centrosomal Loci in Neurons

We have shown a large *Nin* alternative exon 18 (>2,000 nt) that is almost exclusively included in mouse and human NPCs but skipped in neurons (Figures 2J and 2K; ΔPSI = −83.5%). In contrast, we also identified a conserved 61-nt exon (exon 29) of *Nin* that is specifically included in neurons (CP) but skipped in NPCs (Figures 3C and 3D; ΔPSI = 74.0%), introducing a frameshift and truncating the C terminus of Nin (Figures 3E and 3F). Nin associates with the mother centriole to anchor microtubules, with its C-terminal segment targeting efficiently to centrosomes (Delgehyr et al., 2005). Although Nin translocates from centrosome to non-centrosomal loci during brain progenitor cell differentiation, the underlying mechanism remains unknown (Baird et al., 2004; Ohama and Hayashi, 2009).

We examined the effects of exon 18 and exon 29 on Nin subcellular localization and found that the C-terminal centrosome-localization signal of Nin (Nin-NPC-CT) is lost with the inclusion of alternative exon 29, causing the neuronal Nin isoform (Nin-Neuron) to be diffusely localized in cytoplasm when highly expressed (Figures 3F and 3G), associating with microtubules at non-centrosomal loci (Figures S3D–S3F). Targeted co-immunoprecipitation (co-IP) screen of centrosomal proteins allowed us to uncover that the Nin-NPC-CT specifically pulled down CEP250 (Figure 3H), and CEP250 knockdown disrupted the centrosomal localization of Nin (Figures 3I and S3G). We further found that CEP170 preferentially interacts with Nin-NPC through exon 18, but not the Nin-Neuron isoform (Figures 3H and S3I). Given that CEP170 relies on Nin for its centrosomal localization (Graser et al., 2007), our data suggest that the Nin-CEP170 interaction is mediated by Nin exon18 and is dynamically regulated by AS. These results indicate a 2-fold AS mechanism: (1) inclusion of neuronal exon 29 dissociates Nin from CEP250 and centrosome, causing Nin to adopt a non-centrosomal localization in neurons, and (2) skipping of Nin exon 18 further dissociates CEP170 from Nin in neurons.

Endogenous Nin-Neuron is significantly elevated in postmitotic neurons during cortical neurogenesis (Figures S4A and S4B). Ectopic expression of Nin-Neuron, but not Nin-NPC, led to significant neural progenitor depletion from the VZ (Figures 4A and 4B) and defective neuronal migration into the CP (Figure S4C). We performed pair-cell assays and found Nin-Neuron expression causes significantly more NPCs to become neurons compared to control or the Nin-NPC isoform (Figures 4C and 4D). Expression of Nin-Neuron disperses endogenous Nin and Dctn1—a key dynactin subunit mediating cytoplasmic dynein-cargo binding—from the centrosome (Figures 4E and 4F), suggesting a dominant negative mechanism in regulating cell fate.

(G–I) Cartoon illustrations of alternatively spliced genes involved in NPC proliferation (G), radial neuronal migration (H), and neuronal differentiation (I).

(J) RNA-seq reads of human *NIN* gene in GW13–16 VZ and CP (left), showing that the 2,139-bp alternative exon is included in VZ (shaded in light blue). Red bars indicate mutations associated with microcephaly, one of which lies in the AS exon (Dauber et al., 2012). The black arrows here and in all following genome browser figures indicate the direction of gene transcription.

(K) qRT-PCR results show that the 2,121-bp mouse homologous *Nin* exon is included in VZ but skipped in non-VZ cells. Data are represented as mean ± SEM.

(L) RNA-seq reads of human *ANK2* gene showing the 6,255-bp alternative exon (shaded) is included in CP. Red bars indicate mutations associated with autism spectrum disorder, two of which lie in the AS exon (Iossifov et al., 2014).

(M) qRT-PCR analysis showing that the mouse homologous *Ank2* exon of (L) is included in non-VZ and skipped in VZ. Data are represented as mean ± SEM.

See also Figure S2 and Tables S1 and S2.

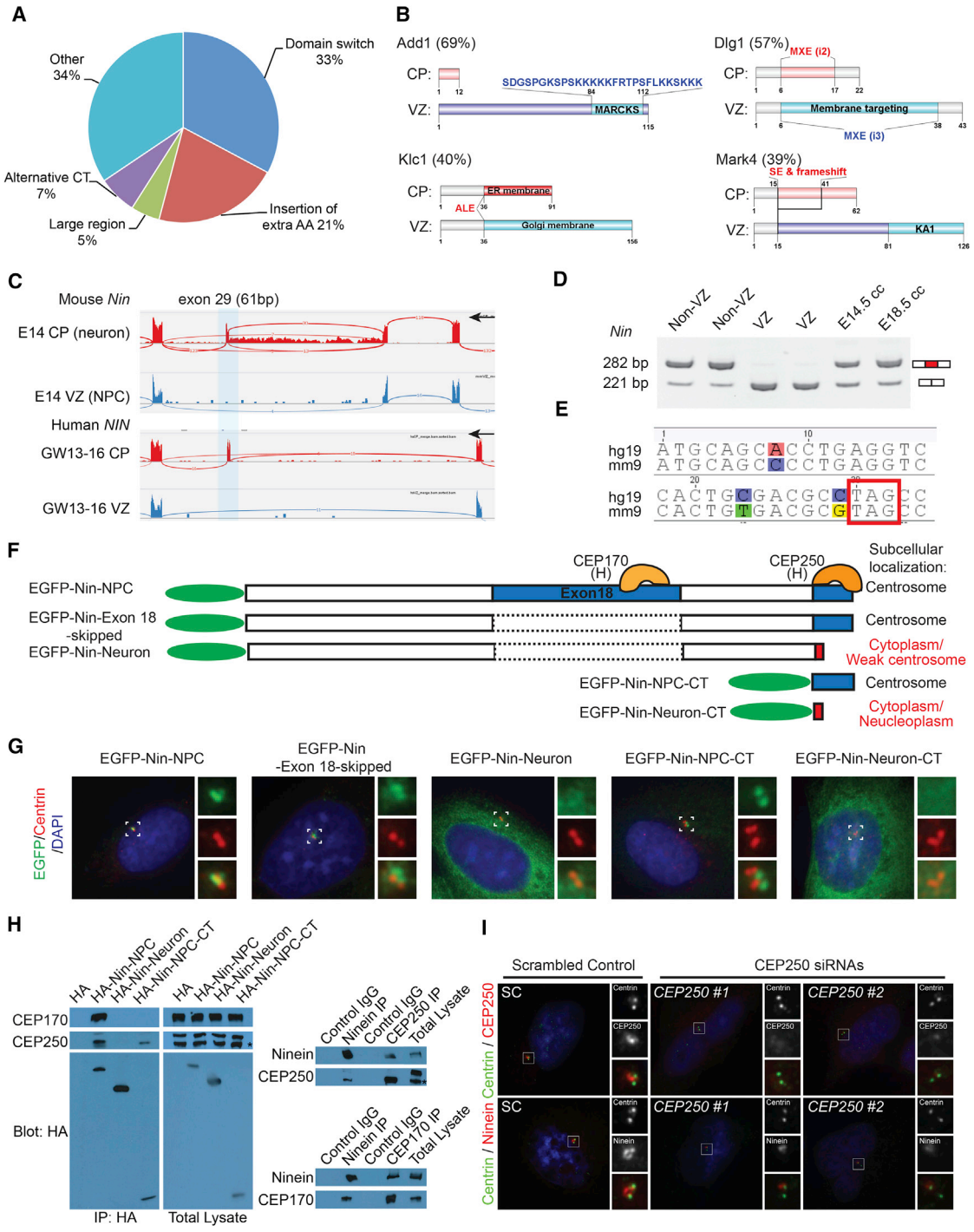

Figure 3. Cell-Type-Specific Alternative Splicing Translocates Ninein from Centrosome in NPCs to Non-centrosomal Loci in Neurons

(A) Impact of 61 cytoskeleton-related and conserved AS events on modular protein domains. AA, amino acids; CT, C terminus.

(B) Alternative splicing alters protein domains that regulate subcellular localization. Gene names are followed by ΔPSI values. Differential protein domains are shaded red (neuron) or cyan (NPC).

(C) RNA-seq reads in E14.5 mouse VZ and CP and GW13–16 human VZ and CP showing that the alternative *Nin* (*NIN*) exon 29 is specifically included in neurons (CP).

(D) RT-PCR validates the specific inclusion of *Nin* exon 29 in differentiating neurons.

(E) Alignment of *Nin* exon 30, showing that insertion of exon 29 introduces a conserved premature stop codon.

(F and G) Cartoon illustration of EGFP-Nin fusion constructs and their subcellular localization in transfected cells.

(legend continued on next page)

We thus created a *NIN* knockout cell line (Chr14:51,259,547delT (hg19), p.Arg107Thrfs*16; Figure S4D) and found that loss of centrosomal NIN disrupted normal mitotic cleavage planes (Figures 4G and 4H). These results indicate that endogenous switching of Nin-NPC to the Nin-Neuron isoform is sufficient to convert cortical NPCs to neurons, suggesting that neurogenesis is normally controlled at least in part by AS of Nin.

Aberrant Splicing of a Cryptic Poison Exon Causes a Unique Brain Malformation

Splicing analysis identified a highly conserved, but not previously annotated, 57-nt exon in *Flna* that is skipped in E14.5 NPCs (VZ) and most adult tissues but included in mRNAs from E14.5 neurons (CP) as well as adult cortex and cerebellum (Figure 5A). Surprisingly, an in-frame stop codon was embedded in this neuron-specific *Flna* exon (Figures 5B and S5A), inclusion of which causes early truncation of Flna protein (482 of 2,647 amino acids; Figure 5C) and/or nonsense-mediated mRNA decay (NMD) (Figure 5D). We thus name the *Flna* SE "exonN" (N stands for null in neuron) and found that the human homologous exonN is skipped in VZ whereas included in CP (Figure 5E). The skipping of exonN in cortical NPCs creates a full-length protein, whereas splicing into this exon in neurons would give a truncated protein or unstable mRNA. Remarkably, genomic sequences of this exon, including the embedded stop codon, are conserved across multiple placental mammalian species, though it is not observed outside mammals (Figure 5F).

The presence of poison exons encoding translational stop codons reported here and by other groups (Yan et al., 2015) suggests a potential mechanism of human disease that, to our knowledge, has not been previously described: mutations that disrupt normal suppression of a poison exon would inactivate protein expression in a cell that normally skips the exon. We tested this model by studying *FLNA*, because heterozygous null mutations in females typically cause periventricular nodular heterotopia (PVNH), where neurons form nodules along the VZ, reflecting failure of normal migration (Fox et al., 1998). We hypothesized that, because abnormal inclusion of exonN will create a *FLNA* null allele (Figures 5B–5F), mutations that promote exonN inclusion in NPCs may lead to PVNH.

Sequencing *FLNA* exonN and its flanking introns in 221 individuals with genetically unexplained PVNH revealed a rare variant *FLNA-as* (ChrX: 153,594,210 C>T, hg19, c.1429+182 G>A) in a large family in which multiple individuals show PVNH that is notably milder than that caused by *FLNA*-null alleles (Figures 5G–5I). Unlike typical females with heterozygous *FLNA*-null mutations, who have abnormally located neurons lining the entire lateral ventricles bilaterally, the PVNH in *FLNA-as* patients is striking but limited to smaller segments of the VZ, often asymmetrically (Figure 5G). The *FLNA-as* mutation lies in the upstream intron of exonN (Figure 5J) and leads to abnormal exonN inclusion in patient blood cells, where exonN is normally skipped (Figure 5K). Furthermore, *FLNA*-null mutations are usually male lethal, yet affected males in this family do not show early lethality. Males and females with null *FLNA* mutations also show variably penetrant congenital heart disease and severe vascular catastrophes (Fox et al., 1998), but the *FLNA-as* pedigree shows no significant cardiovascular disease, suggesting that the *FLNA-as* mutation may cause a brain-specific and cell-type-specific phenotype.

We expressed wild-type (WT) and mutated *FLNA* mini-genes in Neuro2a cells (Figures 5J, 5L, and 5M) and in E14.5 mouse cortical NPCs (Figure 5N) and found that the WT mini-gene produced transcripts that skipped exonN (PSI < 5%), whereas the mini-gene with the *FLNA-as* mutation produced 40%–50% of *FLNA* transcripts that abnormally included exonN or the last 8 nt of exonN that creates a frameshift (Figures 5L, 5N, and S5B). *FLNA-as* mutation led to a truncated FLNA mini-protein and reduced levels of mini-proteins (Figure 5M). These results confirm that the c.1429+182 G>A mutation promoted abnormal exonN inclusion in NPCs, creating a cell-type- and tissue-specific FLNA partial loss of function and an atypical PVNH syndrome.

Ptbp1 and Rbfox1/2/3 Antagonistically Regulate Neuronal Exon Inclusion in the Developing Cerebral Cortex

We used DREME (Bailey, 2011) to identify discriminative *cis*-regulatory sequence motifs enriched in the flanking introns of cassette exons that are preferentially included in neurons. The only two significant motifs identified correspond to binding motifs of Ptbp1/2 (CU(C/U)UCUU; found within 200 nt in the upstream intron; p value = 3.6e−9) and Rbfox1/2/3 (GCAU(G/A); within 200 nt in the downstream intron; p value = 1.3e−8; Figure 6A). Notably, 61% of alternatively spliced neuronal exons had Ptbp1/2 and/or Rbfox1/2/3 regulatory motifs (Figure S6A). Analyses of Rbfox HITS-CLIP and Ptbp1 iCLIP datasets from neuronal samples (Linares et al., 2015; Weyn-Vanhentenryck et al., 2014) further support that many cortically regulated exons exhibit direct binding by these proteins (Figure S6B; Table S4; below).

It has been shown that Ptbp1 binding upstream suppresses exon inclusion (Keppetipola et al., 2012), whereas Rbfox binding downstream enhances exon inclusion (Kuroyanagi, 2009; Wang et al., 2008). We found that *Ptbp1* mRNAs and proteins were highly expressed in NPCs (VZ), with *Rbfox1*/2/3 specifically expressed in neurons (CP; Figures 6B and S6C), consistent with the positional enrichment around neuron-specific exons. Knockdown of Ptbp1, but not Ptbp2, de-repressed inclusion of predicted neuronal exons, including *Flna* exonN (Figures 6C, 6D, S6D, and S6E), and resulted in decreased Flna protein expression (Figure 6E). Moreover, the protein levels of Ptbp1 and Flna were high in E12.5 mouse cortex and dropped over similar time courses during cortical development (Figure S6F). Analysis of Ptbp1 iCLIP-seq datasets (Linares et al., 2015; Masuda et al., 2012) revealed that Ptbp1 bound to the alternatively spliced *Flna* exonN in both NPCs and C2C12 cells (Figure 6F).

(H) (Left) Co-IP of transfected Ninein isoforms showing that Nin-NPC, but not the Nin-Neuron isoform, pulls down CEP170 and CEP250. (Right) Co-IP showing that endogenous Ninein interact with CEP170 and CEP250 in HeLa cells.
(I) siRNA knockdown of CEP250 disrupts the centrosomal localization of Ninein.
See also Figure S3 and Table S3.

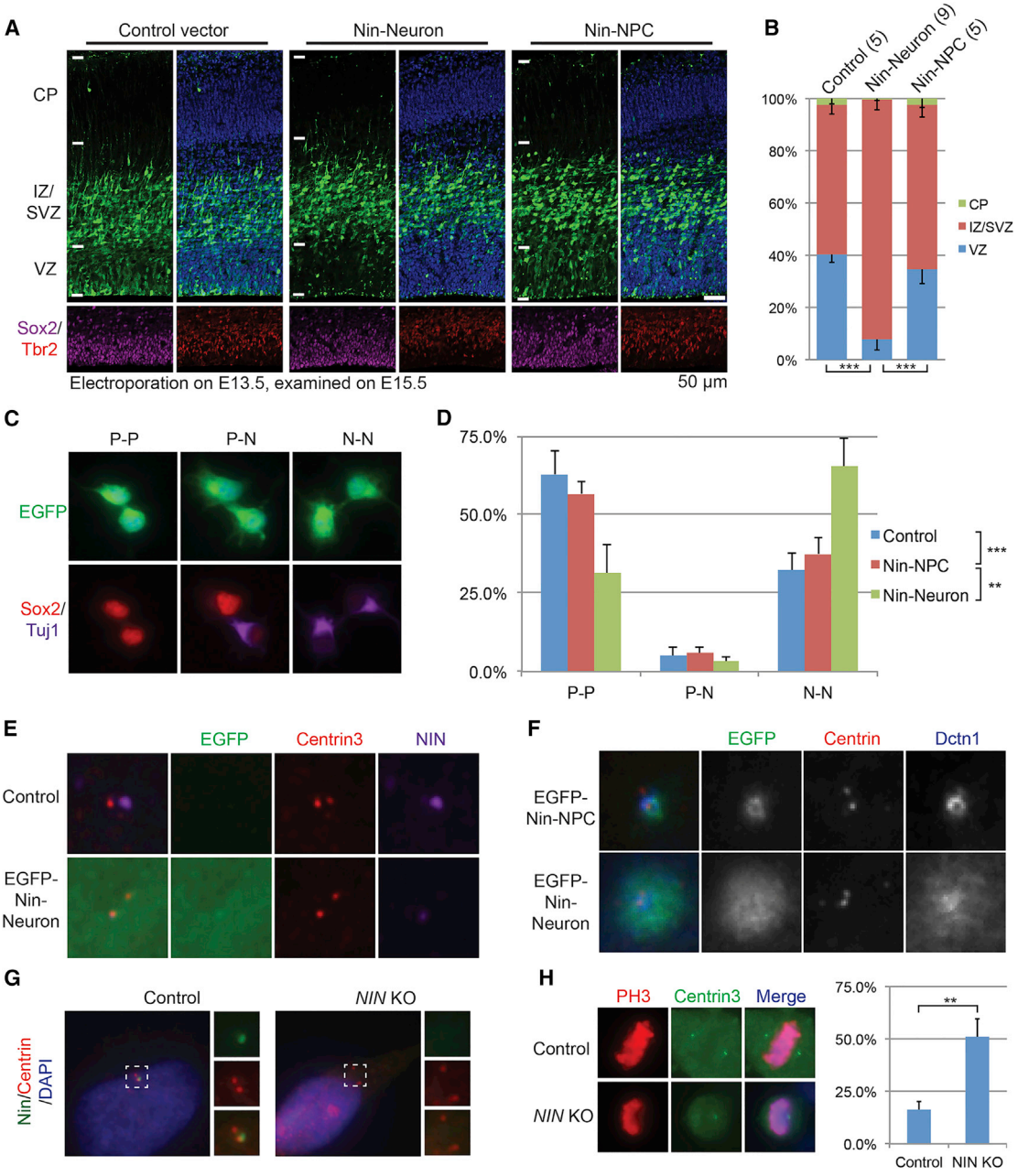

Figure 4. Ninein Neuronal Isoform Promotes NPC Differentiation

(A and B) Expressing Nin-Neuron, but not the Nin-NPC isoform, in E13.5 mouse brains leads to fewer NPCs in the VZ at E15.5. Numbers in parentheses indicate the number of embryos (n) analyzed. Data are represented as mean ± SD.

(C and D) Pair-cell analyses showing that expression of Nin-Neuron promotes neuron production. P, progenitor; N, neuron. Data are represented as mean ± SD.

(E) Expression of Nin-Neuron isoform decreases the level of endogenous NIN at the centrosome.

(F) Expression of Nin-Neuron disperses Dctn1 away from centrosome.

(G) NIN signal is diminished in *NIN* knockout cells.

(H) *NIN* loss of function leads to defective mitotic spindles. Data are represented as mean ± SD.

See also Figure S4.

The mouse homologous nucleotide (chrX:71,486,253, mm9) of the PVNH-associated *FLNA* c.1429+182 G>A mutation lies within a Ptbp1 iCLIP cluster (Figure 6F), suggesting that the human mutation disrupts splicing regulation via PTBP1.

Expression of Rbfox1/2/3 proteins significantly promoted inclusion of predicted neuronal exons (Figures 6G, S6G, and S6H), especially *Nin* exon 29 (Figure 6H), which led to decreased endogenous Ninein at the centrosome (Figure 6I). Re-analysis of

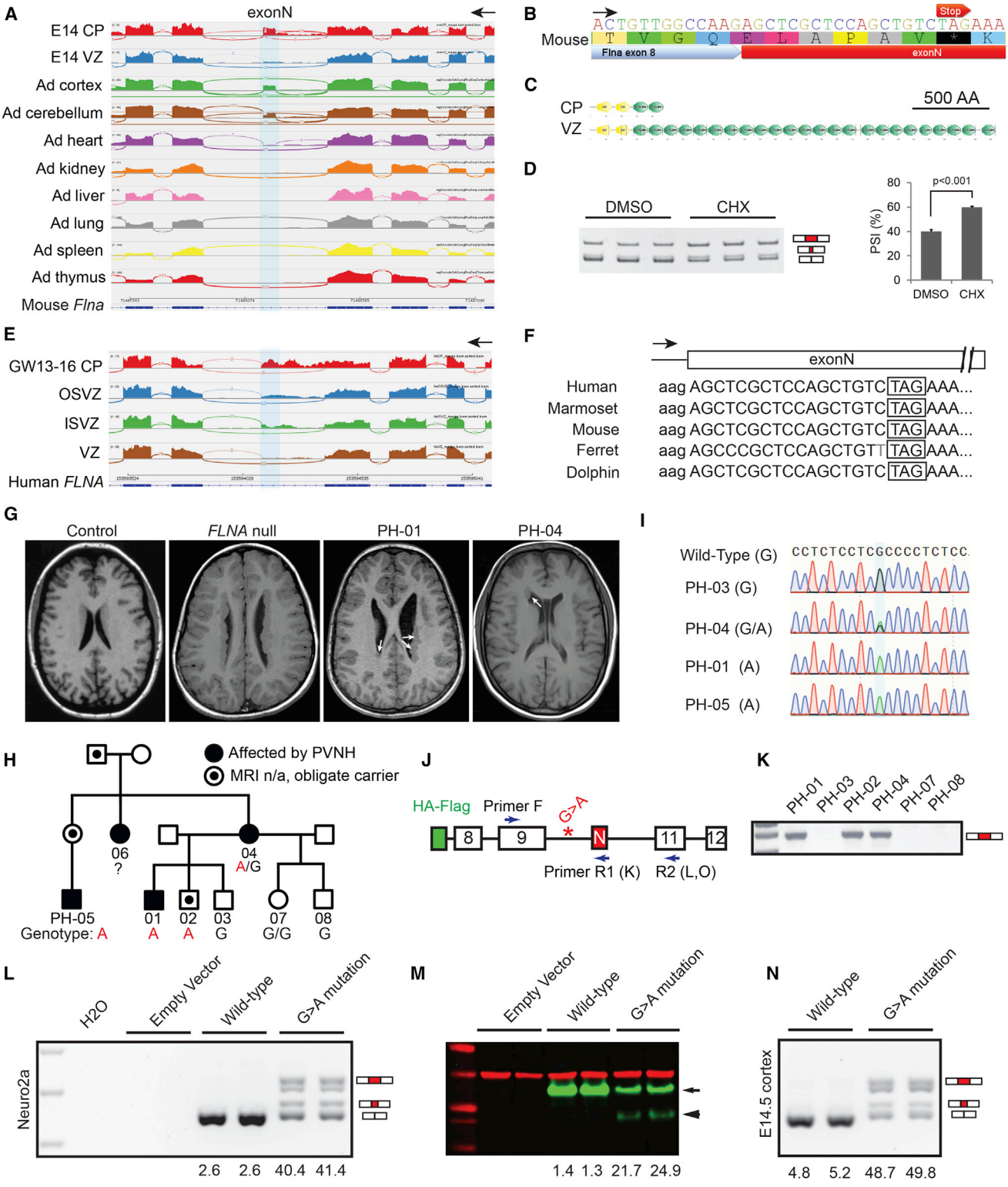

Figure 5. Cell-Type-Specific Alternative Splicing of Filamin A in Cerebral Cortical Development and Human PVNH

(A) RNA-seq reads around *Flna* exonN showing its higher inclusion in adult cerebral cortex, cerebellum, and E14.5 CP, in comparison to E14.5 VZ and other non-neural adult tissues.

(B) *Flna* exonN has an in-frame stop codon.

(C) ExonN inclusion is predicted to truncate Flna protein.

(legend continued on next page)

Rbfox-1/2/3 HITS-CLIP datasets from P15 mouse brains (Weyn-Vanhentenryck et al., 2014) revealed that Rbfox1 and Rbfox3 bound to a conserved GCAUG motif and Rbfox2 CLIP tags mapped to a different but adjacent GCAUG motif (Figures 6J and S6I). These results indicate that Rbfox proteins bind to the downstream intron of *Nin* exon 29 and promote exon inclusion. In summary, Ptbp1 in NPCs suppresses splicing of a family of neuronal exons, including *Flna* exonN, whereas Rbfox1/2/3 in neurons promotes inclusion of over 120 neuronal exons, including *Nin* exon 29. Thus, Ptbp1 and Rbfox1/2/3 proteins antagonistically regulate neuronal exon inclusion during the NPC-to-neuron transition in vivo.

Rbfox Proteins and Ptbp1 Antagonistically Regulate Neurogenesis in Cerebral Cortical Development

Conditional knockout (cKO) of *Ptbp1* in mouse cerebral cortex causes NPCs to detach from the VZ and differentiate prematurely, leading to lethal hydrocephalus, but the pathogenic mechanism and direct downstream targets remain unknown (Shibasaki et al., 2013). We found that *Ptbp1* cKO strikingly phenocopied human PVNH caused by *FLNA* mutations (Figure 7A) and that protein levels of both Flna and its paralog Flnb were significantly decreased in *Ptbp1* knockout cells (Figure 7B). *Flna* exonN was skipped in controls but abnormally included in *Ptbp1* cKO (Figure 7C). We identified an unannotated 98-nt exon of *Flnb* in the homologous location to *Flna* exonN, and this *Flnb* exon was also aberrantly included in Ptbp1 cKO (Figure 7C) and is predicted to cause a translational reading frameshift. These results indicate that Ptbp1 represses inclusion of *Flna* and *Flnb* poison exons in NPCs, and Ptbp1 loss-of-function leads to decreased Flna/Flnb levels and PVNH.

FLNA mutations cause PVNH in humans (Fox et al., 1998), and *Flna* knockout mice show microcephaly, defective adherens junctions, and reduced cortical progenitors (Feng et al., 2006; Lian et al., 2012). To test whether Flna functions downstream of Ptbp1, we knocked down Ptbp1 in E13.5 mouse cortical progenitors and found this led to fewer NPCs in the VZ due to abnormal cell cycle exit (Figures 7D, 7E, and S7A–S7C). Introduction of exogenous *FLNA* by in utero electroporation (IUE) partially rescued the premature NPC depletion phenotype (Figures 7D and 7E), supporting the model that Ptbp1 functions upstream of Flna in cortical neurogenesis.

Ptbp1 represses neuronal fate in tissue culture cells (Xue et al., 2013), and we found that Ptbp1 expression in the developing mouse cortex was highly correlated with Sox2 (Figure S7D). Sox2 is a master transcriptional regulator of NPC identity, and indeed, Sox2 bound to the highly active *Ptbp1* promoter region in NPCs (main peak = 398 nt; fold enrichment = 7.6; p value = 1.0e−16; Figure S7E), suggesting that *Ptbp1* is an important target of Sox2 in suppressing neuronal differentiation.

Single knockout of *Rbfox1* or *Rbfox2* causes minimal structural malformation in mouse cerebral cortex, possibly due to gene redundancy (Gehman et al., 2011, 2012). However, of particular interest is the consequence of Rbfox1/2/3 gain of function in NPCs, because Rbfox proteins promote neuronal exon inclusion and have long been used as pan-neuronal markers. Ectopic expression of Rbfox proteins in NPCs not only significantly decreased the number of VZ NPCs but also dramatically reduced the number of neurons in the CP (Figures 7F and 7G). Furthermore, combining Rbfox3 expression with Ptbp1 knockdown led to a more-severe depletion of VZ NPCs (Figures 7F and 7G). These data indicate that Rbfox1/2/3 and Ptbp1 antagonistically regulate neurogenesis in the developing cerebral cortex (Figure 7H).

DISCUSSION

Here, we show that widespread alternative exon usage during the NPC-to-neuron transition in vivo is critical for mouse and human brain development. Neuronal fate and neuronal exon inclusion are antagonistically regulated by Ptbp1 and Rbfox1/2/3, which are expressed in NPCs and neurons, respectively. Whereas Rbfox1/2/3-induced splicing causes Nin to be translocated from the centrosome in NPCs to non-centrosomal loci in neurons, the expression of Ptbp1 is required for apical progenitor lamination through maintaining Flna and Flnb expression in NPCs.

Perhaps most remarkable in our study is the fact that two opposite and extreme AS events in a single target gene, Ninein, appear sufficient to differentiate NPCs to neurons by removing CEP170- and CEP250-binding domains/exons. This AS mechanism of Nin may also explain previously described microtubule re-organization phenomena during epidermal differentiation

(D) Blocking of NMD by cycloheximide (CHX) in primary hippocampal neurons cultured in vitro for 1 day increases inclusion of exonN. Data are represented as mean ± SEM.
(E) RNA-seq reads showing the inclusion of exonN and retention of its upstream intron in fetal human CP.
(F) Filamin A exonN is conserved across representative placental mammals.
(G) T1 brain MRI shows PVNH (white arrows) in affected individuals PH-01 (male) and PH-04 (female), compared to a healthy control and an unrelated individual with a *FLNA*-null mutation.
(H) Pedigree showing inheritance of PVNH and the rare c.1429 +182 G>A mutation.
(I) Sanger sequencing traces showing the rare *FLNA* variant c.1429+182 G>A.
(J) A cartoon illustrating the *FLNA* mini-gene construct and primers used for RT-PCR. N-terminal HA and Flag tags were fused in frame with exon 8.
(K) RT-PCR using primer F and R1 (inside exonN) detecting the abnormal exonN inclusion in blood samples of affected individuals.
(L) RT-PCR (primer pair F-R2) results on *FLNA* mini-genes expressed in Neuro2a cells, showing that the c.1429+182 G>A mutation caused >40% of *FLNA* transcripts to include exonN.
(M) Western blot of transfected Neuro2a cells detecting the WT mini-FLNA (green, arrow) and the truncated form (arrowhead). Red, anti-Gapdh.
(N) RT-PCR (primer pair F-R2) results of E14.5 mouse brains electroporated *FLNA* mini-genes on E13.5, showing that the G>A mutation caused abnormal inclusion of exonN.
See also Figure S5.

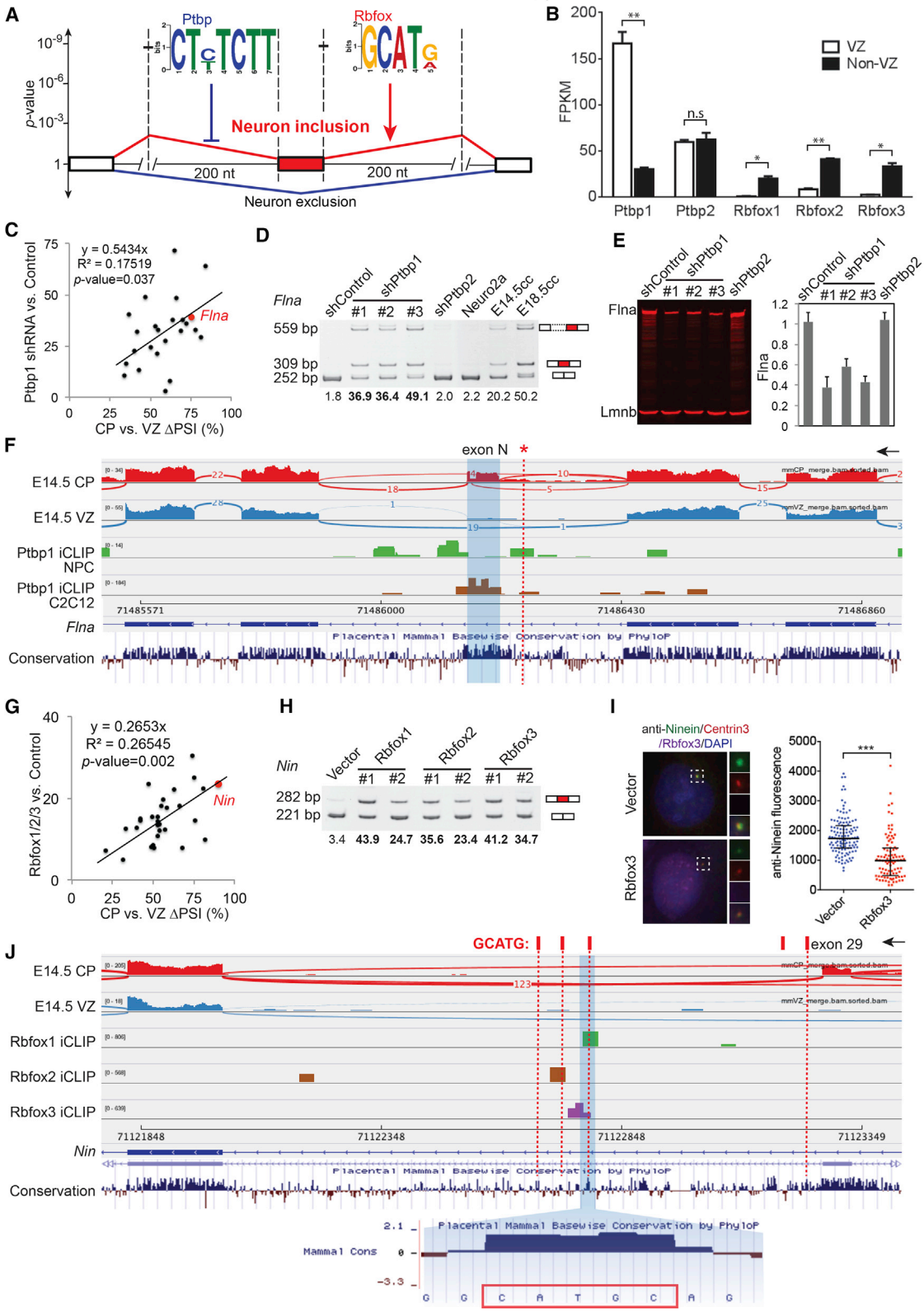

(legend on next page)

(Lechler and Fuchs, 2007) and could potentially regulate epidermal differentiation itself. Whereas our unbiased motif analysis revealed the robust enrichment of Ptbp1/2- and Rbfox1/2/3-binding sequences flanking neuronal exons during the NPC-to-neuron transition, other RBPs may synergistically regulate neuronal exon usage in a context-dependent manner. ELAVL, NOVA, nSR100, and STAR proteins have been reported to regulate specific AS events during cerebral cortical development (Calarco et al., 2009; Darnell, 2013; Iijima et al., 2011), and some of these factors are also differentially expressed between cortical NPCs and neurons.

To our surprise, the brain-specific *Ptbp1* knockout is a mouse model for PVNH (Figure 7A; Shibasaki et al., 2013). Whereas *FLNA* mutations were linked to human PVNH 2 decades ago, *Flna* knockout mice only recapitulate the cardiovascular defects in human patients but do not exhibit PVNH (Feng et al., 2006), likely due to redundant functions of *Flnb*. *Ptbp1* loss disrupts both Flna and Flnb, causing radial glia to detach from the apical surface and forming PVNH. These results demonstrate the essential roles of the Ptbp1-filamin axis in maintaining NPCs and neuroepithelial structure.

As expected from the cell-type-specific splicing of *FLNA*, the intronic *FLNA-as* mutation de-represses exonN inclusion and leads to a unique presentation of PVNH with milder non-CNS manifestations, suggesting the preferential use of this alternative-splicing mechanism in brain. The homologous nucleotide of the *FLNA* c.1429+182 G>A mutation lies within a Ptbp1 iCLIP cluster (Figure 6F), suggesting that the human mutation disrupts splicing regulation via PTBP1. In agreement with this, a computational model of Ptbp1 binding based on iCLIP clusters reported that interspersed G residues are well tolerated but that A residues always impair Ptbp1 binding (Han et al., 2014).

This study reveals that cell-type-specific AS—frequently associated with alternative stop codons and NMD—is widespread in the CNS at early developmental stages and provides functional insights into developmental roles for some of these alternative exons and their upstream splicing regulators. The active usage of many other cell-type-specific poison exons demonstrates not only the demand for larger efforts in genetic testing of their flanking non-coding elements but also the potential of uncovering more master splicing regulators that may play important roles in neurological disorders.

STAR★METHODS

Detailed methods are provided in the online version of this paper and include the following:

- KEY RESOURCES TABLE
- CONTACT FOR REAGENT AND RESOURCE SHARING
- EXPERIMENTAL MODEL AND SUBJECT DETAILS
  - Mouse Maintenance
  - Human Subjects
  - Isolation of Primary Cells from the Developing Mouse Cerebral Cortex
  - Tissue Culture Cells
- METHOD DETAILS
  - RNA Sequencing Analysis
  - Alternative Splicing Analysis
  - Motif Analysis
  - Chip-Seq Analysis
  - Molecular Cloning
  - Protein Analysis
  - In Utero Electroporation
- QUANTIFICATION AND STATISTICAL ANALYSIS
- DATA AND SOFTWARE AVAILABILITY
  - Data Resources

SUPPLEMENTAL INFORMATION

Supplemental Information includes seven figures and six tables and can be found with this article online at http://dx.doi.org/10.1016/j.cell.2016.07.025.

AUTHOR CONTRIBUTIONS

X.Z. conceived and developed the project and performed most wet-lab and bioinformatics experiments. X.W. assisted in MISO analyses and performed RNA motif search. M.H.C. recruited PVNH cases. A.K. and J.F.R. performed Ninein co-IP and related IF. J.F. and P.V.K. analyzed single-cell RNA-seq data with advice from X.Z. R.D. assisted in screening *FLNA* mutations. M.O. and N.Y. provided Ptbp1 cKO samples. J.M. tested reagents. D.L.B. and P.A.S provided guidance on splicing and iCLIP analyses. X.Z. and C.A.W. designed the study and wrote the paper with input from all authors.

Figure 6. Alternative Exons Showing Higher Inclusion in Neurons Are Antagonistically Regulated by Ptbp1 and Rbfox1/2/3 Proteins

(A) Unbiased motif analysis of alternative exons with higher inclusion in differentiating neurons reveals the enrichment of CU(C/U)UCUU in the 200-nt 5′ upstream region and GCAU(G/A) in the 200-nt downstream intronic region.

(B) RNA-seq results of sorted E14.5 mouse cortical cells showing that *Ptbp1* is enriched in NPCs (VZ) and *Rbfox1*/2/3 transcripts are enriched in non-VZ cells. Data are represented as mean ± SEM.

(C) A scatterplot showing that *Ptbp1* knockdown in Neuro2a cells de-represses the inclusion of 24 neuronal exons predicted by motif search in (A).

(D) RT-PCR analysis showing that *Ptbp1* knockdown in Neuro2a cells by three different short hairpin RNAs (shRNAs) promotes inclusion of *Flna* exonN.

(E) Western blot and quantified signals showing that *Ptbp1* knockdown decreases Flna protein level. Data are represented as mean ± SEM.

(F) iCLIP-seq (re-analysis of Linares et al., 2015 and Masuda et al., 2012) and RNA-seq results showing that Ptbp1 binds directly to *Flna* exonN and its flanking introns in NPCs and C2C12 cells. Red asterisk and dotted line indicate chrX:71,486,253 (mm9), the homologous nucleotide of human ChrX: 153,594,210 C>T (hg19) mutation. The arrow indicates direction of transcription.

(G) Rbfox1/2/3 expression in Neuro2a cells promotes inclusion of 30 neuronal exons identified by motif analyses in (A).

(H) RT-PCR results showing that ectopic expression of *Rbfox1*/2/3 promotes inclusion of *Nin* exon 29.

(I) Overexpression of Rbfox3 in U2OS cells decreases the protein level of centrosomal Nin (green). Data are represented as median ± SD.

(J) Genome browser views of RNA-seq and HITS-CLIP reads (re-analysis of Weyn-Vanhentenryck et al., 2014) showing that Rbfox1/2/3 proteins bind to conserved GCAUG motifs downstream of Nin exon 29 in mouse brains. Vertical red bars on top indicate GCATG sequences.

See also Figure S6 and Table S4.

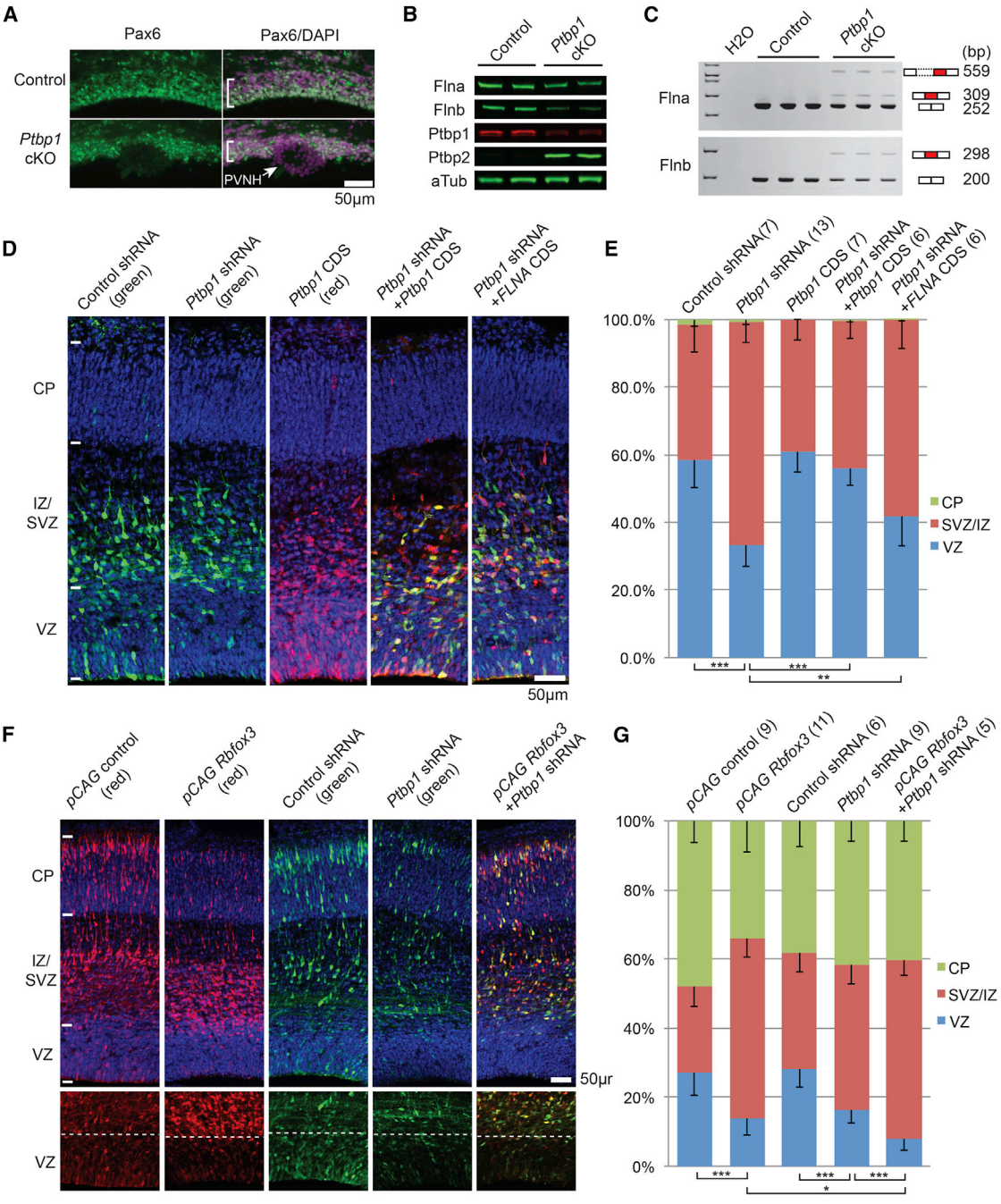

(legend on next page)

ACKNOWLEDGMENTS

We thank B. Barry and J. Partlow for clinical information; Y.J. Yang, A. Lam, D. Gonzalez, and A. Rozzo for technical assistance; M. Bornens, V. Sheen, and G. Lian for reagents; the Orchestra research computing team at Harvard for computing resources; N. Francis of the IDDRC Flow Cytometry Core for technical assistance; and B. Bae, X. Cai, G. Evrony, R.S. Hill, E. Lim, M. Lodato, M. Johnson, and C.A.W. lab members for helpful discussions. We thank Qiufu Ma and Xi He for critical comments on the manuscript. This work was supported by the Manton Center for Orphan Disease Research and grants from the NINDS (R01-NS035129 and R01-NS032457) to C.A.W., NIMH grant (K01-MH109747) and Charles A. King Trust Fellowship to X.Z., HHMI International Student Research Fellowship to X.W., NSF graduate fellowship (DGE1144152) to J.F., NIGMS (R01-GM49662) to D.L.B., and NIGMS (R01-GM34277) and NCI (P01-CA42063) to P.A.S. C.A.W. is an Investigator of the Howard Hughes Medical Institute.

Received: December 22, 2015
Revised: May 22, 2016
Accepted: July 18, 2016
Published: August 25, 2016

REFERENCES

Ayoub, A.E., Oh, S., Xie, Y., Leng, J., Cotney, J., Dominguez, M.H., Noonan, J.P., and Rakic, P. (2011). Transcriptional programs in transient embryonic zones of the cerebral cortex defined by high-resolution mRNA sequencing. Proc. Natl. Acad. Sci. USA *108*, 14950–14955.

Bailey, T.L. (2011). DREME: motif discovery in transcription factor ChIP-seq data. Bioinformatics *27*, 1653–1659.

Baird, D.H., Myers, K.A., Mogensen, M., Moss, D., and Baas, P.W. (2004). Distribution of the microtubule-related protein ninein in developing neurons. Neuropharmacology *47*, 677–683.

Barbosa-Morais, N.L., Irimia, M., Pan, Q., Xiong, H.Y., Gueroussov, S., Lee, L.J., Slobodeniuc, V., Kutter, C., Watt, S., Colak, R., et al. (2012). The evolutionary landscape of alternative splicing in vertebrate species. Science *338*, 1587–1593.

Belgard, T.G., Marques, A.C., Oliver, P.L., Abaan, H.O., Sirey, T.M., Hoerder-Suabedissen, A., García-Moreno, F., Molnár, Z., Margulies, E.H., and Ponting, C.P. (2011). A transcriptomic atlas of mouse neocortical layers. Neuron *71*, 605–616.

Bhalla, K., Phillips, H.A., Crawford, J., McKenzie, O.L., Mulley, J.C., Eyre, H., Gardner, A.E., Kremmidiotis, G., and Callen, D.F. (2004). The de novo chromosome 16 translocations of two patients with abnormal phenotypes (mental retardation and epilepsy) disrupt the A2BP1 gene. J. Hum. Genet. *49*, 308–311.

Calarco, J.A., Superina, S., O'Hanlon, D., Gabut, M., Raj, B., Pan, Q., Skalska, U., Clarke, L., Gelinas, D., van der Kooy, D., et al. (2009). Regulation of vertebrate nervous system alternative splicing and development by an SR-related protein. Cell *138*, 898–910.

Camp, J.G., Badsha, F., Florio, M., Kanton, S., Gerber, T., Wilsch-Bräuninger, M., Lewitus, E., Sykes, A., Hevers, W., Lancaster, M., et al. (2015). Human cerebral organoids recapitulate gene expression programs of fetal neocortex development. Proc. Natl. Acad. Sci. USA *112*, 15672–15677.

Creyghton, M.P., Cheng, A.W., Welstead, G.G., Kooistra, T., Carey, B.W., Steine, E.J., Hanna, J., Lodato, M.A., Frampton, G.M., Sharp, P.A., et al. (2010). Histone H3K27ac separates active from poised enhancers and predicts developmental state. Proc. Natl. Acad. Sci. USA *107*, 21931–21936.

Darnell, R.B. (2013). RNA protein interaction in neurons. Annu. Rev. Neurosci. *36*, 243–270.

Dauber, A., Lafranchi, S.H., Maliga, Z., Lui, J.C., Moon, J.E., McDeed, C., Henke, K., Zonana, J., Kingman, G.A., Pers, T.H., et al. (2012). Novel microcephalic primordial dwarfism disorder associated with variants in the centrosomal protein ninein. J. Clin. Endocrinol. Metab. *97*, E2140–E2151.

Delgehyr, N., Sillibourne, J., and Bornens, M. (2005). Microtubule nucleation and anchoring at the centrosome are independent processes linked by ninein function. J. Cell Sci. *118*, 1565–1575.

Dillman, A.A., Hauser, D.N., Gibbs, J.R., Nalls, M.A., McCoy, M.K., Rudenko, I.N., Galter, D., and Cookson, M.R. (2013). mRNA expression, splicing and editing in the embryonic and adult mouse cerebral cortex. Nat. Neurosci. *16*, 499–506.

Fan, J., Salathia, N., Liu, R., Kaeser, G.E., Yung, Y.C., Herman, J.L., Kaper, F., Fan, J.B., Zhang, K., Chun, J., and Kharchenko, P.V. (2016). Characterizing transcriptional heterogeneity through pathway and gene set overdispersion analysis. Nat. Methods *13*, 241–244.

Feng, Y., Chen, M.H., Moskowitz, I.P., Mendonza, A.M., Vidali, L., Nakamura, F., Kwiatkowski, D.J., and Walsh, C.A. (2006). Filamin A (FLNA) is required for cell-cell contact in vascular development and cardiac morphogenesis. Proc. Natl. Acad. Sci. USA *103*, 19836–19841.

Fietz, S.A., Lachmann, R., Brandl, H., Kircher, M., Samusik, N., Schröder, R., Lakshmanaperumal, N., Henry, I., Vogt, J., Riehn, A., et al. (2012). Transcriptomes of germinal zones of human and mouse fetal neocortex suggest a role of extracellular matrix in progenitor self-renewal. Proc. Natl. Acad. Sci. USA *109*, 11836–11841.

Finn, R.D., Bateman, A., Clements, J., Coggill, P., Eberhardt, R.Y., Eddy, S.R., Heger, A., Hetherington, K., Holm, L., Mistry, J., et al. (2014). Pfam: the protein families database. Nucleic Acids Res. *42*, D222–D230.

Fox, J.W., Lamperti, E.D., Ekşioğlu, Y.Z., Hong, S.E., Feng, Y., Graham, D.A., Scheffer, I.E., Dobyns, W.B., Hirsch, B.A., Radtke, R.A., et al. (1998). Mutations in filamin 1 prevent migration of cerebral cortical neurons in human periventricular heterotopia. Neuron *21*, 1315–1325.

Gao, P., Postiglione, M.P., Krieger, T.G., Hernandez, L., Wang, C., Han, Z., Streicher, C., Papusheva, E., Insolera, R., Chugh, K., et al. (2014). Deterministic

Figure 7. Ptbp1 and Rbfox Proteins Antagonistically Control Neural Progenitor Cell Differentiation

(A) Immunostaining of E18.5 *Ptbp1* conditional knockout (cKO) (*Nestin-Cre*) cerebral cortex showing typical PVNH (white arrow) and thinner ventricular layer of Pax6+ cells (brackets).

(B) Western blot of *Ptbp1* cKO and control mouse embryonic fibroblast (MEF) cells showing that proteins level of Ptbp1, Flna, and Flnb are decreased in *Ptbp1* cKO, whereas Ptbp2 level is increased.

(C) RT-PCR results showing that *Ptbp1* cKO in MEF cells de-represses the inclusion of *Flna* exonN and a 98-nt *Flnb* exon.

(D and E) Representative images and statistical analysis (E) showing that *Ptbp1* knockdown (green) at E13.5 results in reduced neural progenitors in the VZ at E15.5. The defect was partially rescued by co-expression of *Ptbp1* coding sequence (CDS) (red) or *FLNA* CDS. Numbers in parentheses indicate the number of embryos analyzed. Data are represented as mean ± SD.

(F and G) Representative images and statistical analysis (G) showing that introducing Rbfox3 expression into E13.5 mouse brains resulted in reduced progenitor cells in the VZ and reduced neurons in the CP at E16.5. Ectopic expression of Rbfox3 on top of *Ptbp1* knockdown causes a more-severe depletion of NPCs in the VZ. Data are represented as mean ± SD.

(H) A working model showing that Rbfox1/2/3 proteins are highly expressed in neurons and promote neuronal exon inclusion (red), whereas Ptbp1 is expressed in NPCs (blue, VZ) and represses neuronal exon inclusion. Sox2 binds to the promoter region of Ptbp1 (left). Dysregulation of Rbfox1/2/3-mediated AS may lead to brain disorders, such as autism and intellectual disability. Mutations that de-repress neuronal exon inclusion in NPCs may result in PVNH (through *FLNA*).

See also Figure S7.

progenitor behavior and unitary production of neurons in the neocortex. Cell *159*, 775–788.

Gehman, L.T., Stoilov, P., Maguire, J., Damianov, A., Lin, C.H., Shiue, L., Ares, M., Jr., Mody, I., and Black, D.L. (2011). The splicing regulator Rbfox1 (A2BP1) controls neuronal excitation in the mammalian brain. Nat. Genet. *43*, 706–711.

Gehman, L.T., Meera, P., Stoilov, P., Shiue, L., O'Brien, J.E., Meisler, M.H., Ares, M., Jr., Otis, T.S., and Black, D.L. (2012). The splicing regulator Rbfox2 is required for both cerebellar development and mature motor function. Genes Dev. *26*, 445–460.

Gong, S., Zheng, C., Doughty, M.L., Losos, K., Didkovsky, N., Schambra, U.B., Nowak, N.J., Joyner, A., Leblanc, G., Hatten, M.E., and Heintz, N. (2003). A gene expression atlas of the central nervous system based on bacterial artificial chromosomes. Nature *425*, 917–925.

Graser, S., Stierhof, Y.D., Lavoie, S.B., Gassner, O.S., Lamla, S., Le Clech, M., and Nigg, E.A. (2007). Cep164, a novel centriole appendage protein required for primary cilium formation. J. Cell Biol. *179*, 321–330.

Greig, L.C., Woodworth, M.B., Galazo, M.J., Padmanabhan, H., and Macklis, J.D. (2013). Molecular logic of neocortical projection neuron specification, development and diversity. Nat. Rev. Neurosci. *14*, 755–769.

Han, A., Stoilov, P., Linares, A.J., Zhou, Y., Fu, X.D., and Black, D.L. (2014). De novo prediction of PTBP1 binding and splicing targets reveals unexpected features of its RNA recognition and function. PLoS Comput. Biol. *10*, e1003442.

Huang da, W., Sherman, B.T., and Lempicki, R.A. (2009). Systematic and integrative analysis of large gene lists using DAVID bioinformatics resources. Nat. Protoc. *4*, 44–57.

Huttner, W.B., Kelava, I., and Lewitus, E. (2013). Progenitor networking in the fetal primate neocortex. Neuron *80*, 259–262.

Iijima, T., Wu, K., Witte, H., Hanno-Iijima, Y., Glatter, T., Richard, S., and Scheiffele, P. (2011). SAM68 regulates neuronal activity-dependent alternative splicing of neurexin-1. Cell *147*, 1601–1614.

Iossifov, I., O'Roak, B.J., Sanders, S.J., Ronemus, M., Krumm, N., Levy, D., Stessman, H.A., Witherspoon, K.T., Vives, L., Patterson, K.E., et al. (2014). The contribution of de novo coding mutations to autism spectrum disorder. Nature *515*, 216–221.

Irimia, M., Weatheritt, R.J., Ellis, J.D., Parikshak, N.N., Gonatopoulos-Pournatzis, T., Babor, M., Quesnel-Vallières, M., Tapial, J., Raj, B., O'Hanlon, D., et al. (2014). A highly conserved program of neuronal microexons is misregulated in autistic brains. Cell *159*, 1511–1523.

Johnson, M.B., Kawasawa, Y.I., Mason, C.E., Krsnik, Z., Coppola, G., Bogdanović, D., Geschwind, D.H., Mane, S.M., State, M.W., and Sestan, N. (2009). Functional and evolutionary insights into human brain development through global transcriptome analysis. Neuron *62*, 494–509.

Johnson, M.B., Wang, P.P., Atabay, K.D., Murphy, E.A., Doan, R.N., Hecht, J.L., and Walsh, C.A. (2015). Single-cell analysis reveals transcriptional heterogeneity of neural progenitors in human cortex. Nat. Neurosci. *18*, 637–646.

Katz, Y., Wang, E.T., Airoldi, E.M., and Burge, C.B. (2010). Analysis and design of RNA sequencing experiments for identifying isoform regulation. Nat. Methods *7*, 1009–1015.

Kelley, L.A., and Sternberg, M.J. (2009). Protein structure prediction on the Web: a case study using the Phyre server. Nat. Protoc. *4*, 363–371.

Keppetipola, N., Sharma, S., Li, Q., and Black, D.L. (2012). Neuronal regulation of pre-mRNA splicing by polypyrimidine tract binding proteins, PTBP1 and PTBP2. Crit. Rev. Biochem. Mol. Biol. *47*, 360–378.

Kim, D., Pertea, G., Trapnell, C., Pimentel, H., Kelley, R., and Salzberg, S.L. (2013). TopHat2: accurate alignment of transcriptomes in the presence of insertions, deletions and gene fusions. Genome Biol. *14*, R36.

Kuroyanagi, H. (2009). Fox-1 family of RNA-binding proteins. Cell. Mol. Life Sci. *66*, 3895–3907.

Langmead, B., and Salzberg, S.L. (2012). Fast gapped-read alignment with Bowtie 2. Nat Methods *9*, 357–359.

Lechler, T., and Fuchs, E. (2007). Desmoplakin: an unexpected regulator of microtubule organization in the epidermis. J. Cell Biol. *176*, 147–154.

Li, Q., Lee, J.A., and Black, D.L. (2007). Neuronal regulation of alternative pre-mRNA splicing. Nat. Rev. Neurosci. *8*, 819–831.

Li, Y.I., Sanchez-Pulido, L., Haerty, W., and Ponting, C.P. (2015). RBFOX and PTBP1 proteins regulate the alternative splicing of micro-exons in human brain transcripts. Genome Res. *25*, 1–13.

Lian, G., Lu, J., Hu, J., Zhang, J., Cross, S.H., Ferland, R.J., and Sheen, V.L. (2012). Filamin a regulates neural progenitor proliferation and cortical size through Wee1-dependent Cdk1 phosphorylation. J. Neurosci. *32*, 7672–7684.

Linares, A.J., Lin, C.H., Damianov, A., Adams, K.L., Novitch, B.G., and Black, D.L. (2015). The splicing regulator PTBP1 controls the activity of the transcription factor Pbx1 during neuronal differentiation. eLife *4*, e09268.

Lodato, M.A., Ng, C.W., Wamstad, J.A., Cheng, A.W., Thai, K.K., Fraenkel, E., Jaenisch, R., and Boyer, L.A. (2013). SOX2 co-occupies distal enhancer elements with distinct POU factors in ESCs and NPCs to specify cell state. PLoS Genet. *9*, e1003288.

Lui, J.H., Hansen, D.V., and Kriegstein, A.R. (2011). Development and evolution of the human neocortex. Cell *146*, 18–36.

Masuda, A., Andersen, H.S., Doktor, T.K., Okamoto, T., Ito, M., Andresen, B.S., and Ohno, K. (2012). CUGBP1 and MBNL1 preferentially bind to 3′ UTRs and facilitate mRNA decay. Sci. Rep. *2*, 209.

Merkin, J., Russell, C., Chen, P., and Burge, C.B. (2012). Evolutionary dynamics of gene and isoform regulation in Mammalian tissues. Science *338*, 1593–1599.

Ohama, Y., and Hayashi, K. (2009). Relocalization of a microtubule-anchoring protein, ninein, from the centrosome to dendrites during differentiation of mouse neurons. Histochem. Cell Biol. *132*, 515–524.

Raj, B., and Blencowe, B.J. (2015). Alternative splicing in the mammalian nervous system: recent insights into mechanisms and functional roles. Neuron *87*, 14–27.

Raj, B., O'Hanlon, D., Vessey, J.P., Pan, Q., Ray, D., Buckley, N.J., Miller, F.D., and Blencowe, B.J. (2011). Cross-regulation between an alternative splicing activator and a transcription repressor controls neurogenesis. Mol. Cell *43*, 843–850.

Robinson, J.T., Thorvaldsdottir, H., Winckler, W., Guttman, M., Lander, E.S., Getz, G., and Mesirov, J.P. (2011). Integrative genomics viewer. Nat Biotechnol. *29*, 24–26.

Saito, T. (2006). In vivo electroporation in the embryonic mouse central nervous system. Nat. Protoc. *1*, 1552–1558.

Sebat, J., Lakshmi, B., Malhotra, D., Troge, J., Lese-Martin, C., Walsh, T., Yamrom, B., Yoon, S., Krasnitz, A., Kendall, J., et al. (2007). Strong association of de novo copy number mutations with autism. Science *316*, 445–449.

Shen, Q., Zhong, W., Jan, Y.N., and Temple, S. (2002). Asymmetric Numb distribution is critical for asymmetric cell division of mouse cerebral cortical stem cells and neuroblasts. Development *129*, 4843–4853.

Shibasaki, T., Tokunaga, A., Sakamoto, R., Sagara, H., Noguchi, S., Sasaoka, T., and Yoshida, N. (2013). PTB deficiency causes the loss of adherens junctions in the dorsal telencephalon and leads to lethal hydrocephalus. Cereb. Cortex *23*, 1824–1835.

Thorvaldsdottir, H., Robinson, J.T., and Mesirov, J.P. (2013). Integrative Genomics Viewer (IGV): high-performance genomics data visualization and exploration. Brief Bioinform. *14*, 178–192.

Trapnell, C., Roberts, A., Goff, L., Pertea, G., Kim, D., Kelley, D.R., Pimentel, H., Salzberg, S.L., Rinn, J.L., and Pachter, L. (2012). Differential gene and transcript expression analysis of RNA-seq experiments with TopHat and Cufflinks. Nat. Protoc. *7*, 562–578.

Vuong, C.K., Black, D.L., and Zheng, S. (2016). The neurogenetics of alternative splicing. Nat. Rev. Neurosci. *17*, 265–281.

Wang, E.T., Sandberg, R., Luo, S., Khrebtukova, I., Zhang, L., Mayr, C., Kingsmore, S.F., Schroth, G.P., and Burge, C.B. (2008). Alternative isoform regulation in human tissue transcriptomes. Nature *456*, 470–476.

Weyn-Vanhentenryck, S.M., Mele, A., Yan, Q., Sun, S., Farny, N., Zhang, Z., Xue, C., Herre, M., Silver, P.A., Zhang, M.Q., et al. (2014). HITS-CLIP and integrative modeling define the Rbfox splicing-regulatory network linked to brain development and autism. Cell Rep. *6*, 1139–1152.

Xue, Y., Ouyang, K., Huang, J., Zhou, Y., Ouyang, H., Li, H., Wang, G., Wu, Q., Wei, C., Bi, Y., et al. (2013). Direct conversion of fibroblasts to neurons by reprogramming PTB-regulated microRNA circuits. Cell *152*, 82–96.

Yan, Q., Weyn-Vanhentenryck, S.M., Wu, J., Sloan, S.A., Zhang, Y., Chen, K., Wu, J.Q., Barres, B.A., and Zhang, C. (2015). Systematic discovery of regulated and conserved alternative exons in the mammalian brain reveals NMD modulating chromatin regulators. Proc. Natl. Acad. Sci. USA *112*, 3445–3450.

Zhang, Y., Liu, T., Meyer, C.A., Eeckhoute, J., Johnson, D.S., Bernstein, B.E., Nusbaum, C., Myers, R.M., Brown, M., Li, W., et al. (2008). Model-based analysis of ChIP-Seq (MACS). Genome Biol. *9*, R137.

STAR★METHODS

KEY RESOURCES TABLE

REAGENT or RESOURCE	SOURCE	IDENTIFIER
Antibodies		
Mouse monoclonal anti-BrdU	Dako	Cat#M0744; RRID: AB_10013660
Rabbit polyclonal anti-Flag	Cell Signaling Technology	Cat#2368S; RRID: AB_10694612
Mouse monoclonal anti-Flag (M2)	Sigma-Aldrich	Cat#F3165; RRID: AB_259529
Rabbit polyclonal anti-Flna	Epitomics	Cat#2242-1
Mouse monoclonal anti-Gapdh	Abcam	Cat#ab8245; RRID: AB_2107448
Rat monoclonal anti-HA	Roche	Cat#11867423001; RRID: AB_10094468
Rat monoclonal anti-Histone H3 (S28p)	Sigma-Aldrich	Cat#H9908; RRID: AB_260096
Rabbit polyclonal anti-Ki67	Abcam	Cat#15580; RRID: AB_443209
Goat polyclonal anti-Lamin B	Santa Cruz	Cat#sc-6217; RRID: AB_648158
Rabbit polyclonal anti-Ninein	Bethyl	Cat#A301-504A; RRID: AB_999627
Goat polyclonal anti-Ptbp1	Abcam	Cat#ab5642; RRID: AB_305011
Mouse monoclonal anti-Ptbp1	Life technologies	Cat#324800
Rabbit polyclonal anti-Ptbp2	Millipore	Cat#ABE431
Mouse monoclonal anti-Rbfox1/A2BP1	Millipore	Cat#MABE159; RRID: AB_10807159
Rabbit polyclonal anti-Rbfox2/RBM9	Bethyl	Cat#A300-864A; RRID: AB_609476
Mouse monoclonal anti-Rbfox3/NeuN	Millipore	Cat#MAB377; RRID: AB_2298772
Goat polyclonal anti-Sox2	Santa Cruz	Cat#sc-17320; RRID: AB_2286684
Rabbit polyclonal anti-Tbr2	Abcam	Cat#ab23345; RRID: AB_778267
Chemicals, Peptides, and Recombinant Proteins		
Cycloheximide	Sigma-Aldrich	Cat#C4859-1ML
EGF	Thermo-Fisher	Cat#PHG0314
FGF2	Thermo-Fisher	Cat#PHG0264
N2	Thermo-Fisher	Cat#17502048
B27	Thermo-Fisher	Cat#17504044
5-Bromo-2-deoxyuridine	Sigma-Aldrich	Cat#B5002
Critical Commercial Assays		
Papain Dissociation System	Worthington	Cat#LK003150
NEXTflex Directional RNA-Seq Kit	Bioo Scientific	Cat#5129-05
Ribo-Zero Magnetic Gold Kit	Epicenter	Cat#MRZG126
Deposited Data		
RNA-Seq	This Paper	GEO: GSE76198
Experimental Models: Cell Lines		
Mouse: Neuro2a	ATCC	Cat#CCL-131
Human: HeLa	ATCC	Cat#CCL-2
Human: U2OS	ATCC	Cat#HTB-96
Human: 293T/17	ATCC	Cat#CRL-11268
Experimental Models: Organisms/Strains		
Tbr2-EGFP transgenic mice	GENSAT Project at Rockefeller University	Tg(Eomes-EGFP)DQ10Gsat
Ptbp1 conditional knockout mice	Shibasaki et al., 2013	$Ptb^{floxed/floxed}$
Recombinant DNA		
See Table S6 for Recombinant DNA (plasmids)		
Sequence-Based Reagents		
See Table S5 for the List of Oligos		

(*Continued on next page*)

Continued

REAGENT or RESOURCE	SOURCE	IDENTIFIER
Software and Algorithms		
Tophat-2.0.7	Kim et al., 2013	https://ccb.jhu.edu/software/tophat/index.shtml
MISO-0.4.6	Katz et al., 2010	http://genes.mit.edu/burgelab/miso/
DREME	Bailey, 2011	http://meme-suite.org/tools/dreme
Bowtie-2.2.4	Langmead and Salzberg, 2012	http://bowtie-bio.sourceforge.net/bowtie2/index.shtml
MACS-2.1.0	Zhang et al., 2008	https://github.com/taoliu/MACS
Integrative Genomics Viewer (IGV)	Robinson et al., 2011; Thorvaldsdottir et al., 2013	https://www.broadinstitute.org/igv/

CONTACT FOR REAGENT AND RESOURCE SHARING

Please contact C.A.W. (christopher.walsh@childrens.harvard.edu) for reagents and resources generated in this study.

EXPERIMENTAL MODEL AND SUBJECT DETAILS

Mouse Maintenance

Mouse protocols were reviewed and approved by Institutional Animal Care and Use Committee (IACUC) at Boston Children's Hospital (BCH) and all colonies were maintained following animal research guidelines at BCH. The *Tbr2-EGFP* transgenic mouse line, for which an *EGFP-PolyA* cassette was inserted in front of the translational start codon in a FVB/NTac mouse stain, was obtained from GENSAT (Gong et al., 2003) and crossed to the FVB inbreed strain for at least two generations. Heterozygous transgenic mice did not display any obvious developmental defects. Dorsal cerebral cortices were dissected from embryonic day 14.5 (E14.5) heterozygous *Tbr2-EGFP* transgenic embryos and pooled for splicing analyses without distinguishing genders.

Human Subjects

All human protocols were reviewed and approved by the institutional review board of BCH. Informed consent was obtained from all subjects involved in this study or from parents of those who were younger than 18 years old. PVNH cases screened in this study were recruited from diverse ethnic groups and a Caucasian pedigree carrying the *FLNA-as* mutation is described. Mutations were detected with DNA extracted from blood samples. Splicing analyses of affected individuals were performed with RNA samples extracted from immortalized lymphoblasts.

Isolation of Primary Cells from the Developing Mouse Cerebral Cortex

Dissected brain tissues are dissociated with the Papain Dissociation System (Worthington). Single cell suspension (Neural Basal medium supplemented with 2% B27, 1% N2, 1% Penicillin Streptomycin (PenStrep), 10ng/ml EGF, 10ng/ml FGF2, 0.5% FBS and 0.25% HEPES) was cooled on ice and immediately sorted on the FACSAria II (BD). For immunostaining, sorted cells were plated in Lab-Tek chamber slides (Thermo) and cultured for 4 hr before fixation.

Tissue Culture Cells

Cell lines including Neuro2a (a neuroblastoma cell line with a NPC-like state), HeLa and Ptbp1 cKO MEF cells were used for transfection (Lipofectamine 2000, Life Tech) or lentiviral transduction. Lentiviral vectors were packaged and infected following the The RNAi Consortium (TRC) protocols. Briefly, the envelop plasmid (pMD2.G, Addgene, 12259), packaging plasmid (psPAX2, Addgene, 12260), and pLKO.1 based vectors were cotransfected into HEK293T/17 (ATCC, CRL-11268), and viral particles were harvested 42 hr post-transfection. Ptbp1 cKO MEF cells were transduced with lentiviral particles carrying control plasmid or CMV-Cre for protein and RNA analyses. To generate *NINEIN* knockout cell line, pX459 (Addgene 48139) carrying guide sequences were transfected into HeLa cells and puromycin (5μg/ml) selected colonies were screened for mutant alleles.

METHOD DETAILS

RNA Sequencing Analysis

Total RNA was extracted using RNeazy Mini Kit (QIAGEN) and treated with Turbo DNase (Ambion). RINs measured by Bioanalyzer (Agilent) for all samples were above 9.0. 500-2000ng total RNA was treated with Ribo-Zero Gold (Epicenter), and mRNA was enriched using Oligo(dT)25 Dynabeads (Life Tech). RNA-Seq libraries (2 replicates each for VZ and non-VZ cells, n or number of embryos = 7 and 11 for VZ, n = 7 and 8 for non-VZ replicates) were prepared using ligation-based directional RNA-Seq kit (Bio Scientific), and

sequenced on Illumina HiSeq2000. 36 to 42 million single reads (50bp) were obtained for each replicate, trimmed, aligned (mm9, Tophat-2.0.7, allowing 2 mismatches) and analyzed using the Tuxedo protocol (Kim et al., 2013; Trapnell et al., 2012). Gene expression levels are presented as FPKM (Fragments Per Kilobase of exon per Million reads). Gene ontology analyses were performed using the DAVID online tools (Huang da et al., 2009).

Alternative Splicing Analysis

Aligned bam files (mm9) were analyzed using MISO (version 0.4.6). PSI values of each non-VZ replicate were compared to each VZ replicate, only alternative splicing events that were consistent across all comparisons were considered for downstream analysis. Additional RNA-Seq datasets of laser microdissected cortical tissues (Ayoub et al., 2011; Fietz et al., 2012) were analyzed using the same pipeline. Sashimi plots of RNA-Seq reads were generated in Integrative Genomics Viewer (IGV) (Robinson et al., 2011; Thorvaldsdottir et al., 2013). To study alternative splicing changes during human brain development, published RNA-Seq datasets (Fietz et al., 2012) on laser microdissected fetal human cortical tissues across GW13-16 were aligned to human genome (hg19) and analyzed using the MISO pipeline. Alternatively spliced human exons ($|\Delta PSI| \geq 10\%$, and Bayes factor ≥ 5) were lifted over to the mouse genome (mm9) and compared to splicing events identified in E14.5 mouse cortex (Figure 1D). RNA-Seq datasets from the ENCODE project were analyzed for tissue distribution of alternative exons.

Motif Analysis

We performed DREME (Bailey, 2011) motif discovery in each of the four regions around differentially spliced cassette exons in mouse: the first 200 nts (i.e., 5′ end) of the upstream intron, the last 200 nts (i.e., 3′ end) of the upstream intron, the first 200 nts of the downstream intron, and the last 200 nts of the downstream intron. For each region, we used exons with higher PSI in neurons as foreground, and exons with higher PSI in NPCs as background, and verse versa. DREME (version 4.9.0) were then run with the option '-norc –e 0.05' to identify significant motifs in each region.

Chip-Seq Analysis

Chip-Seq reads for Sox2 (Lodato et al., 2013) and H3K27ac (Creyghton et al., 2010) on NPCs cultured in vitro were trimmed, and aligned to the mouse genome (mm9) with Bowtie 2.2.4 (Langmead and Salzberg, 2012) allowing zero or one mismatch. Mapped reads were visualized in IGV. Peaks were called using MACS 2.1.0 (Zhang et al., 2008) and statistical results were presented.

Molecular Cloning

pCAGIG (Addgene, 11159) vector and its derivatives were used for ectopic expression of genes in the neuronal system. First, the multiple cloning sites (MCS) between *EcoR I* and *Not I* was replaced with *EcoR I-ATG(start codon)-HA(1x)-Flag(1x)-Asc I-Not I*. Next, the EGFP expression cassette between *Msc I* and *Fse I* was replaced with either an mCherry or Puromycin resistance cassette. Coding or genomic sequences of specific genes (e.g., genomic sequences of WT human *FLNA* between exon 8 and exon 12 and the same sequence carrying the c.1429+182 G>A mutation) were PCR amplified and inserted between *Asc I* and *Not I* sites. To knockdown Ptbp1 and Ptbp2 in Neuro2a cells, oligos were annealed and cloned into pLKO.1 TRC cloning vector (Addgene, 10878) between *EcoR I* and *Age I* sites. To knockdown Ptbp1 expression in mouse brains, effective hairpins tested in Neuro2a cells (#3) and a control hairpin were end-modified and cloned into the pLL3.7 vector (Addgene, 11795) between HpaI and *Xho I* sites. For reverse transcription and polymerase chain reaction (RT-PCR), cDNAs from independent samples were amplified with Phusion (NEB) for 26-30 cycles and analyzed on agarose gels or Novex TBE gels (Life Tech). qRT-PCR (quantitative RT-PCR) were carried out using SYBR Green (ABI). Oligo sequences are listed in Table S5, and plasmids are listed in Table S6.

Protein Analysis

Protein domains were analyzed using Pfam (Finn et al., 2014). 3-D protein structures were predicted on the SWISS-MODEL and Phyre2 servers (Kelley and Sternberg, 2009). Protein lysates were resolved on SDS-PAGE gels and Western Blots were carried out using the Li-Cor Odyssey system. For immunofluorescence staining (IF), embryonic mouse brains were dissected out, fixed in 4% paraformaldehyde, and coronal sections were obtained using a Vibratome or Cryostat (Leica Biosystems). Tissue sections or fixed tissue culture cells were rinsed twice in 1x PBS with 0.2% Triton X-100 (PBST) and incubated at room temperature in a blocking solution (PBST and 4% normal donkey serum), followed by incubation with primary antibodies at 4°C overnight. Samples were then washed 3 times with PBST and incubated with fluorescence conjugated secondary Alexa antibodies (Life Technologies) at room temperature for 2 hr. Slides were mounted with Fluoromount G (Southern Biotech) and imaged on Imager M2 (Carl Zeiss). Primary antibodies are listed in Key Resource Table.

In Utero Electroporation

In utero electroporation (IUE) was performed following standard protocols (Saito, 2006). In brief, a timed pregnant CD-1 mouse (E13.5) was anesthetized with isoflurane, laid on a 37°C warm plate, the uterine horns exposed and bathed in warm 1x HBSS (1% Pen/Strep), and ~1 μl of plasmid DNA (1-2μg/ μl) mixed with Fast Green was microinjected into the lateral ventricles of embryos using a glass micropipette (Drummond Scientific). Five 50 ms pulses of 30-50 mV at 950-ms intervals were delivered across the uterus with a pair of electrode paddles placed on each side of the embryo's head using a square-pulse electroporator (BTX, ECM 830). Following

electroporation, the uterus was repositioned back into the abdominal cavity and the wound was surgically sutured. The whole process was performed in a sterile environment. After surgery, the animals were closely monitored until they recovered and resumed normal activity. Pair-cell assays were performed following published protocols (Shen et al., 2002). Briefly, in utero electroporated NPCs expressing ectopic Nin isoforms were dissociated, FACS sorted, plated at clonal density and their progeny pair classified as progenitors (Sox2+; Tuj1-), neurons (Sox2-; Tuj1+) or a mixture.

QUANTIFICATION AND STATISTICAL ANALYSIS

Statistical analyses for differential gene expression and splicing changes (Figures 1, 2, and 6) were performed in R and MISO. Levels of significance were calculated with Student's t test for Figure 6I, and with Hypergeometric Test for Figure S6B. Isoform abundance on DNA gels was measured in Photoshop and normalized with DNA length. For statistical analyses of cell fates (Figures 4 and 7), five to thirteen positive embryos were analyzed for each condition (specific numbers of analyzed embryos are indicated in each figure), and three to four sections were examined for each embryo. Percentages presented Figures 4 and 7 were calculated by dividing the number of EGFP+ cells in each zone (eg, VZ, IZ/SVZ and CP) by the total number of EGFP+ cells of all zones on the same images. Percentages of cells in the VZ were compared using one-way ANOVA in GraphPad Prism, and means ± (standard deviation, SD) are presented. In all figures: *, p-value < 0.05; **, p-value < 0.01; ***, p-value < 0.001.

DATA AND SOFTWARE AVAILABILITY

Data Resources

The accession number for the RNA sequencing data reported in this paper is NCBI GEO: GSE76198.

Supplemental Figures

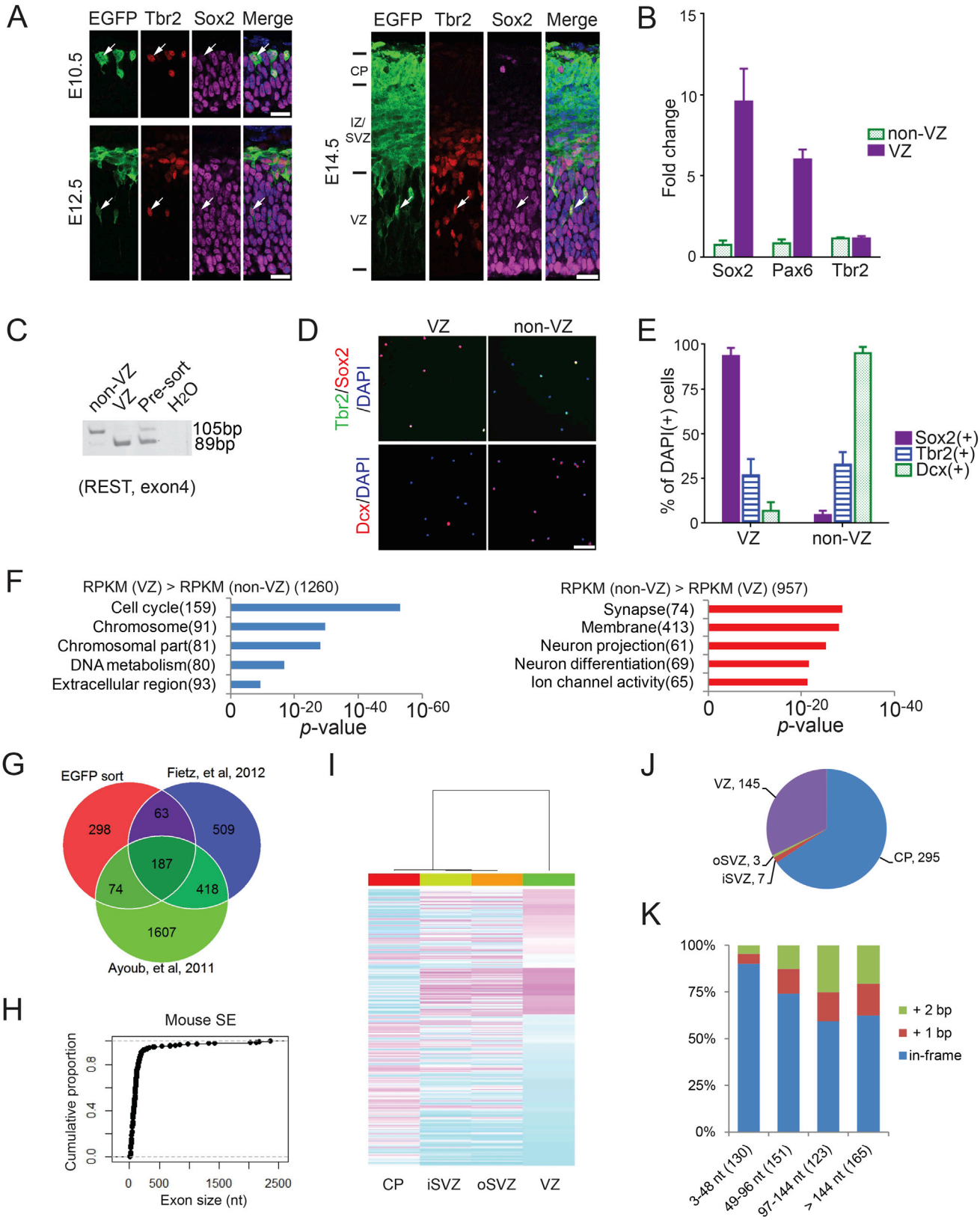

(legend on next page)

Figure S1. RNA-Seq Analysis of NPCs and Neurons Revealed Systematic Alternative Splicing Changes during Neurogenesis in the Developing Cerebral Cortex, Related to Figure 1

(A) Immunostaining of E10.5, E12.5 and E14.5 *Tbr2-EGFP* mouse dorsal cerebral cortex with anti-EGFP (green), anti-Tbr2 (red) and anti-Sox2 (magenta). White arrows indicate that (EGFP+) cells in the VZ/SVZ are (Tbr2+; Sox2-). Scale bar, 20 μm.

(B) Quantitative RT-PCR results showing that *Sox2* and *Pax6* mRNAs are enriched in FACS sorted VZ cells.

(C) RT-PCR results showing that the neuronal exon 4 of REST is enriched in FACS sorted non-VZ cells and depleted from sorted VZ cells.

(D) Immunostaining of FACS sorted VZ and non-VZ cells with anti-Sox2, anti-Tbr2 and anti-DCX. Scale bar, 100 μm.

(E) Statistic analysis of D) showing that sorted VZ cells are mostly Sox2 (+), and that sorted non-VZ cells are Dcx postive.

(F) Gene ontology analysis of differentially expressed genes (over 4 fold difference, $p < 0.01$) showing that cell cycle related genes are overrepresented in sorted VZ cells, and synaptic and neuron differentiation genes are enriched in sorted non-VZ cells.

(G) A Venn diagram showing the number of shared alternative splicing events that we identified in three independent RNA-Seq datasets.

(H) A cumulative dot plot showing the size distribution of mouse SEs.

(I) Heatmap and unsupervised clustering of PSI values for alternative exons (each row or line) between human VZ, iSVZ, oSVZ and CP (magenta represent high PSI value and light blue showing low PSI values).

(J) Pie chart showing alternative exons that are specifically included or skipped in each of VZ, iSVZ, oSVZ and CP samples.

(K) Histograms showing the size of human SEs (x axis) and the percentages of SEs that cause an in-frame insertion or a frameshift (y axis).

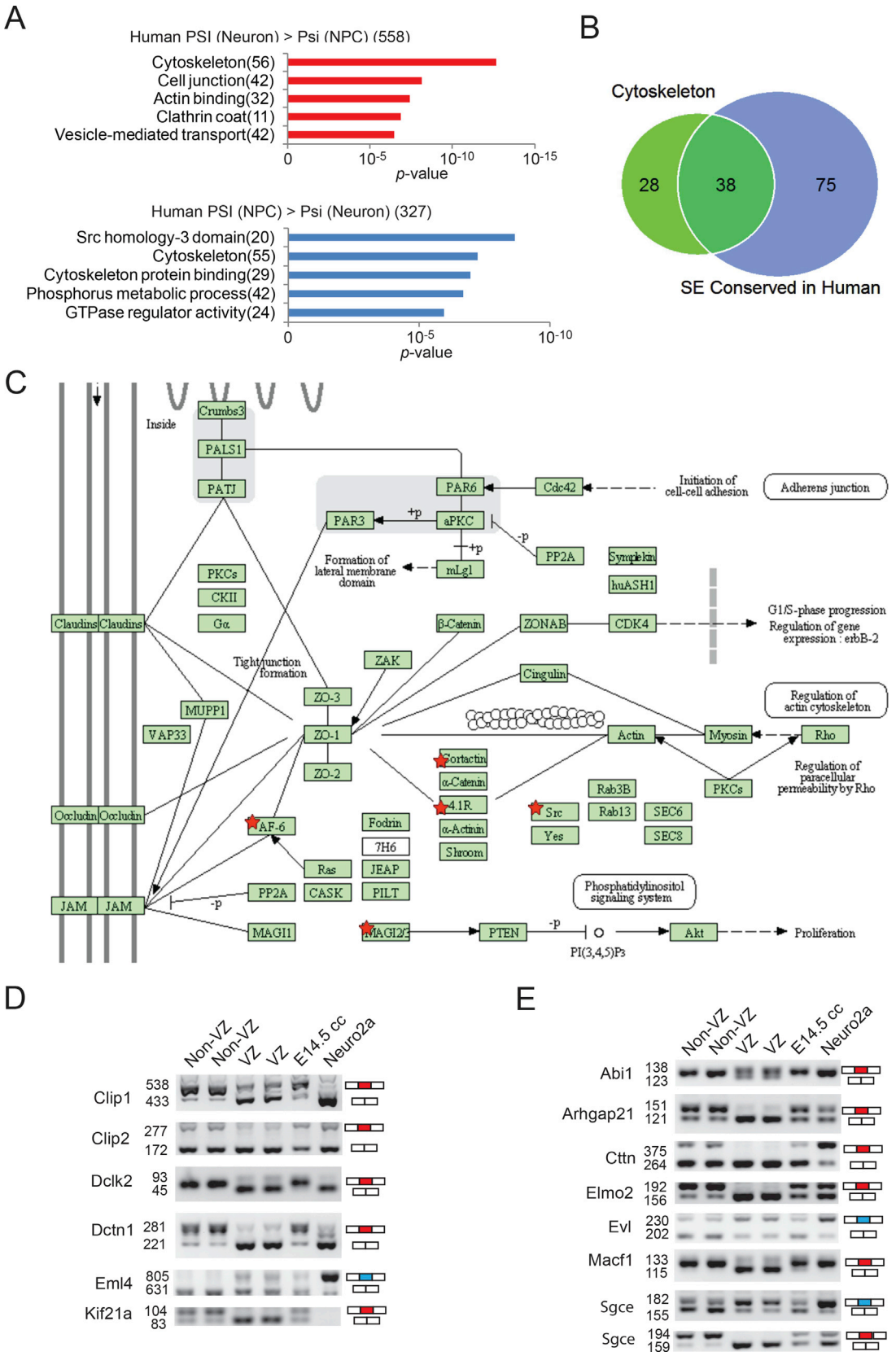

(legend on next page)

Figure S2. Alternative Splicing Preferentially Regulates Genes Encoding Cytoskeleton-Related Proteins during Neurogenesis, Related to Figure 2

(A) Gene ontology analysis of human genes that were differentially spliced between GW13-16 fetal human NPCs and neurons, showing that genes related to cytoskeleton and other biological functions were overrepresented.

(B) A Venn diagram showing that alternative exons in 38 of 66 (58%) cytoskeleton related mouse SEs are also alternatively spliced in the developing human cerebral cortex.

(C) KEGG pathway analysis of alternatively spliced genes revealed their functions (red stars) in regulating tight junctions (p-value = 0.002).

(D and E) Additional RT-PCR analyses of alternatively spliced exons in microtubule- (C) and actin- (D) related genes in mice.

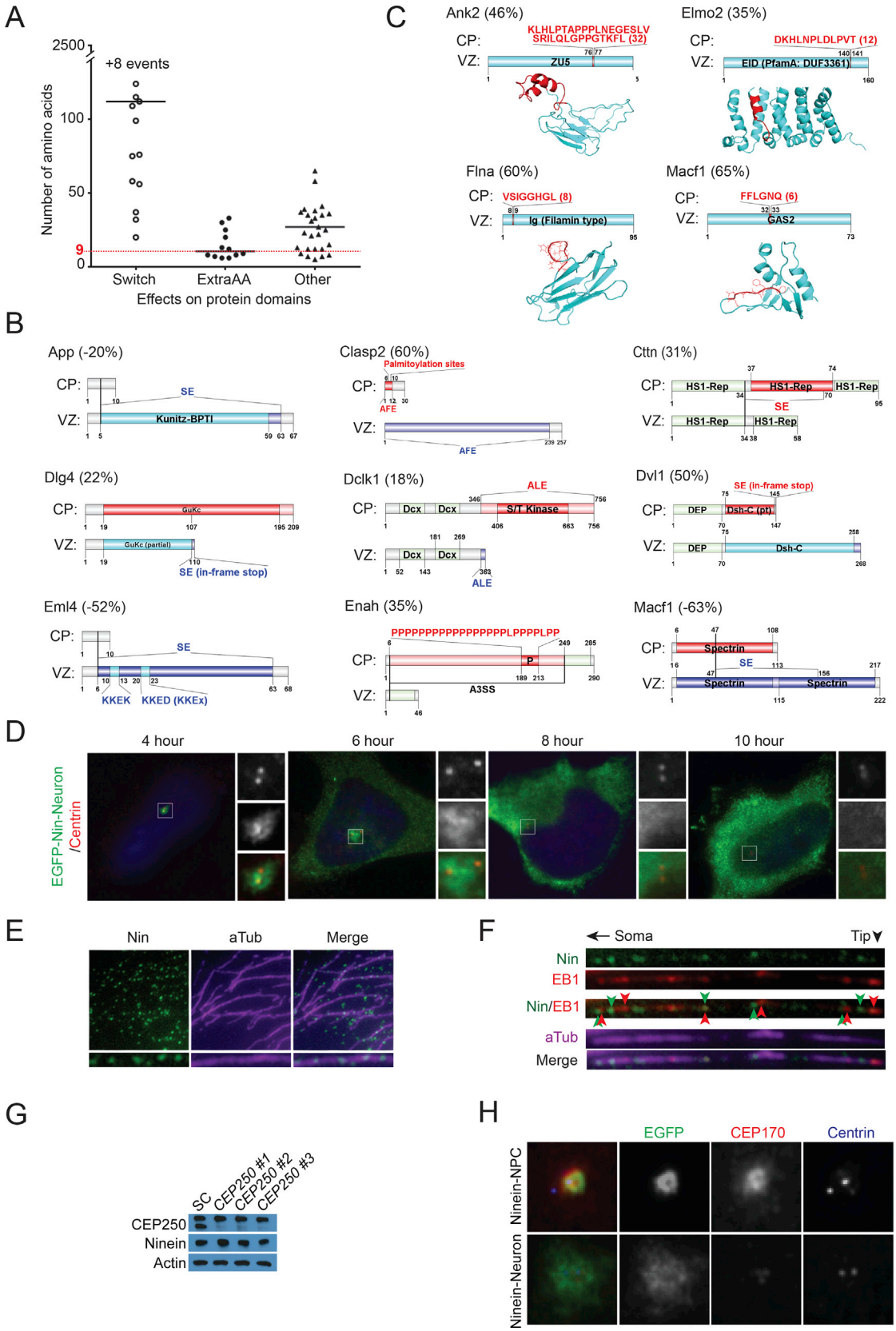

(legend on next page)

Figure S3. Alternatively Spliced Exons during Neurogenesis Critically Alter Protein Structures, Related to Figure 3

(A) Number of amino acids affected by alternative splicing and their impact on protein domains, with bars showing the median size. Note that short SEs including microexons (5 AA or shorter) tend to insert extra AA into protein domains.

(B) Effects of alternative splicing on protein domains. Gene names are followed by ΔPSI values. Differential sequences are colored light red (neuron specific) or light blue (NPC specific). Differential protein domains are shaded red (neuron) or cyan (NPC).

(C) Representative neuron specific cassette exons inserting extra amino acids (red) into defined proteins domains (cyan). Left to right: 32 amino acids insert to the spectrin-binding ZU5 domain of Ank2; 12 amino acids insert to the ELMO inhibitory domain (EID) of Elmo2; 8 amino acids insert into the 15th immunoglobin like repeat of Flna; 6 amino acids insert into the growth-arrest-specific protein 2 (GAS2) domain of Macf1.

(D) Prolonged and high expression of Nin-Neuron isoform diffuses from centrosomal area to cytoplasm.

(E) Endogenous non-centrosomal Nin associates with microtubules in Caco2 cells.

(F) Endogenous Nin localizes to non-centrosomal microtubules in primary mouse hippocampal neurons.

(G) Western blot results showing that siRNAs against *CEP250* efficiently knocked down CEP250 levels.

(H) EGFP-Nin-NPC, but EGFP-Nin-Neuron, co-localizes with CEP170.

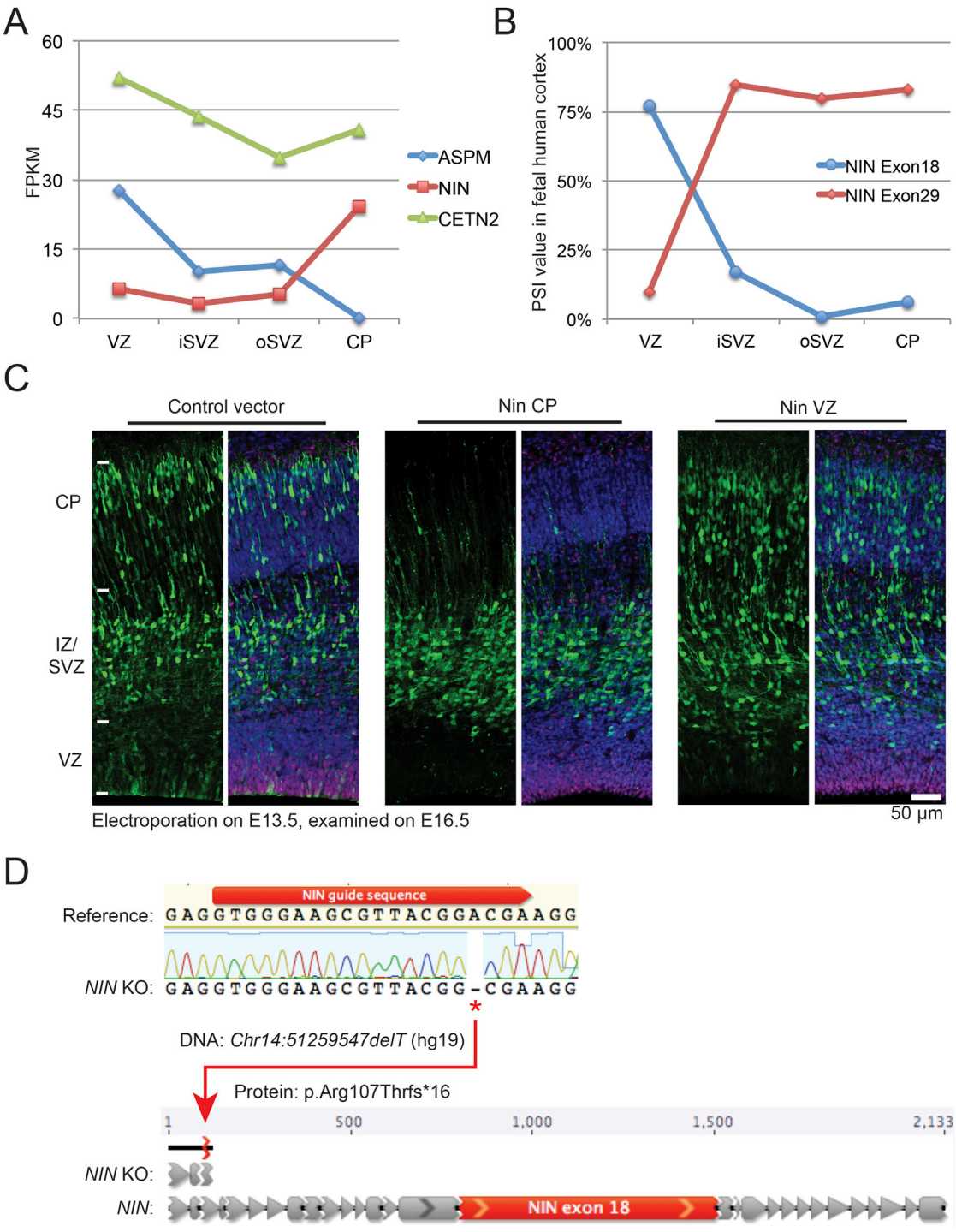

Figure S4. Cell-Type-Specific Alternative Splicing Translocates Ninein from Centrosome in NPCs to Non-centrosomal Loci in Neurons, Related to Figure 4

(A) FPKM values showing that *NIN* expression is higher in CP than in VZ, iSVZ and oSVZ.

(B) PSI values showing that *NIN* exon18 (2139 nt) is specifically included in VZ and the neuronal exon29 (61 nt) is specifically included in other zones.

(C) Introducing the Nin-Neuron isoform, but not the Nin-NPC isoform, into the E13.5 mouse brain leads to fewer NPCs in the VZ and fewer neurons in the CP at E16.5.

(D) The guide sequence used to generate *NIN* knockout cells and the p.Arg107Thrfs*16 early truncation mutation.

Figure S5. Regulation of *Flna* Expression by Alternative Splicing, Related to Figure 5

(A) Alignment of mouse *Flna* and human *FLNA* exonNs (red) and their upstream and downstream exons, showing that the alternative exonNs and the embedded premature stop codons (dashed red line box) are conserved.

(B) Multiple alternatively spliced transcripts around *FLNA* exonN.

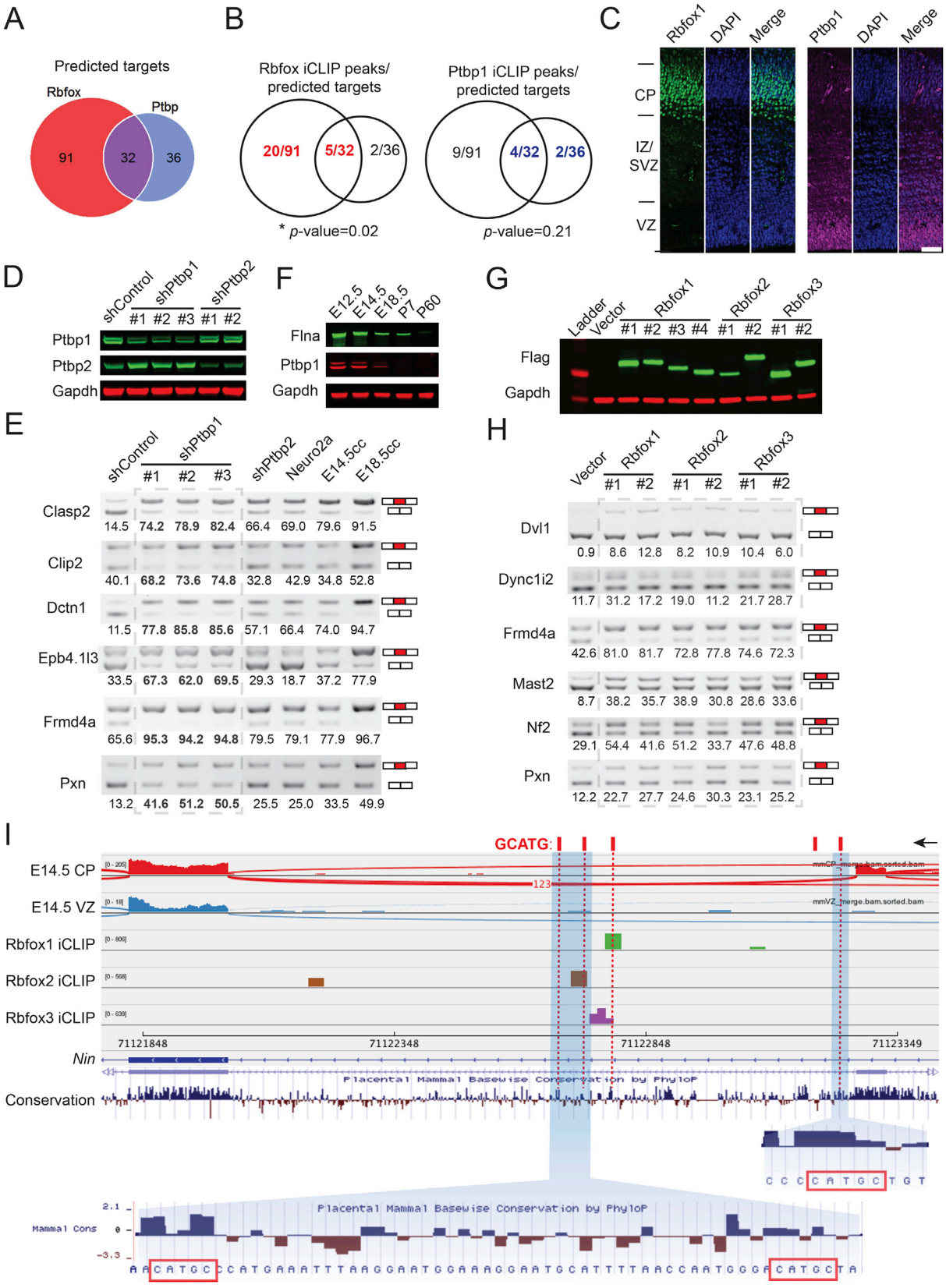

(legend on next page)

Figure S6. The Inclusion of Neuronal Exons Is Regulated by Ptbp1 and Rbfox1/2/3 Proteins, Related to Figure 6

(A) A Venn diagram showing numbers of alternative exons that have upstream Ptbp- and/or downstream Rbfox-binding sites.

(B) Venn diagrams showing Rbfox and Ptbp1 iCLIP peaks associated with predicted targets in A) using previously published iCLIP/HITS-CLIP datasets (Linares et al., 2015; Weyn-Vanhentenryck et al., 2014). .

(C) Immuno-fluorescence staining (green) showing that Rbfox1 is highly expressed in the CP (left), and Ptbp1 (magenta) is specifically expressed in the VZ (right).

(D) Western blot showing that different shRNAs against mouse *Ptbp1* (3) or *Ptbp2* (2) efficiently knock down target protein expression in Neuro2a cells.

(E) RT-PCR analyses showing that *Ptbp1* knockdown promoted the inclusion of neuronal exons, with PSI values shown below.

(F) Western-blot of cerebral cortex lysates showing that the protein levels of Flna and Ptbp1 peaks during early cortex development (E12.5) and drops at later stages.

(G) Western Blot showing ectopic expression of Rbfox1/2/3 isoforms in Neuro2a cells.

(H) RT-PCR analyses show that ectopic expression of *Rbfox1*/2/3 increases neuronal exon inclusion.

(I) HITS-CLIP (re-analysis of datasets reported by an independent study (Masuda et al., 2012)) and RNA-seq results showing that Rbfox1/2/3 proteins bind to conserved GCAUG sequences downstream of Nin exon 29.

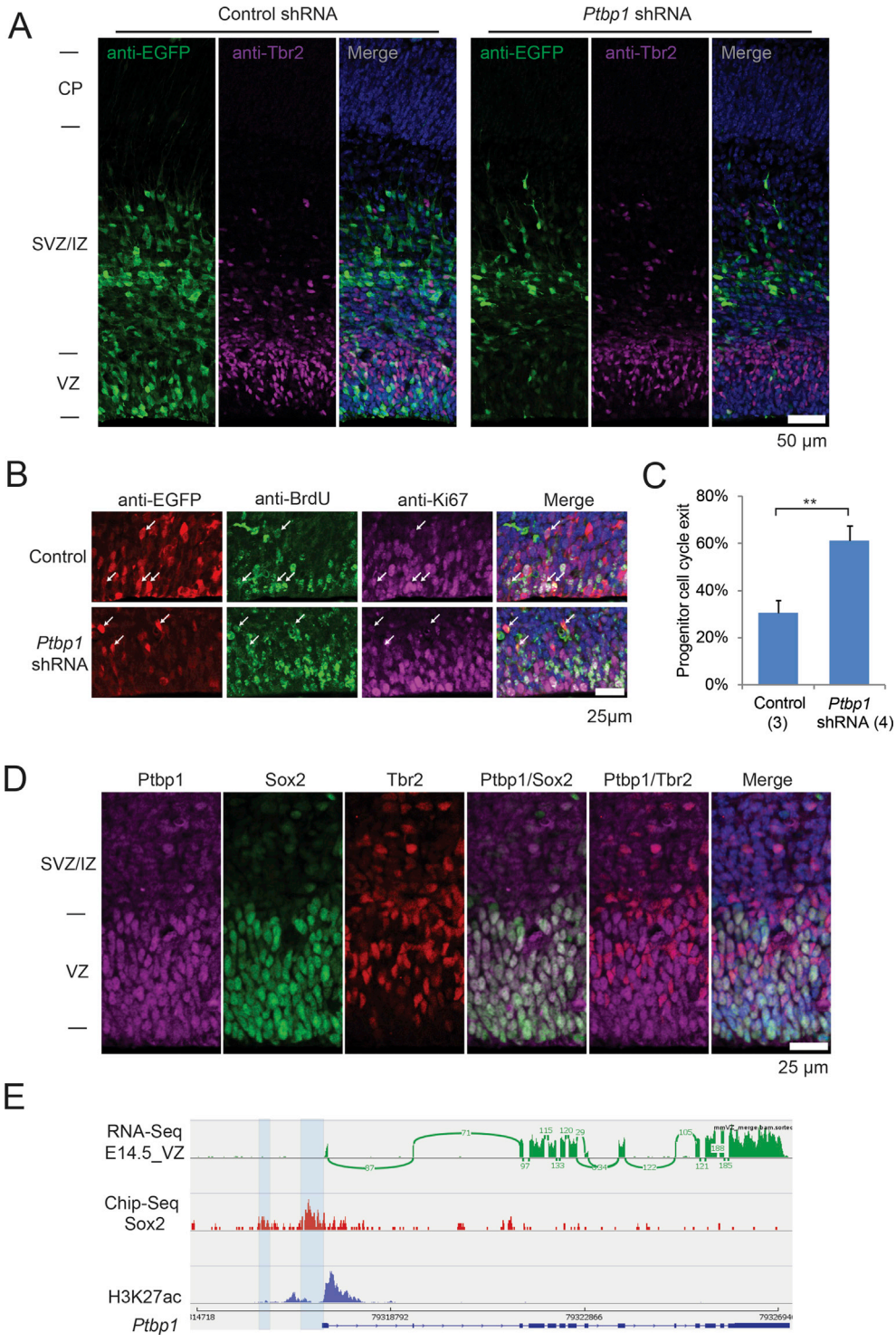

Figure S7. Ptbp1 Is Expressed in NPCs and Maintains the Neural Progenitor Pool, Related to Figure 7

(A) *Ptbp1* shRNA knockdown (anti-EGFP) depleted neural progenitors from VZ.

(B and C) Representative images and statistical analysis (C) showing that *Ptbp1* knockdown (anti-EGFP, red) promotes neural progenitors to exit cell cycle (BrdU+; Ki67-). y axis represents the proportion of (EGFP+; BrdU+; Ki67-) cells over (EGFP+; BrdU+) cells. Data are represented as mean ± SEM.

(D) Ptbp1 co-localizes with Sox2 but not Tbr2 in E14.5 mouse cerebral cortex.

(E) Sox2 and H3K27ac Chip-Seq reads showing that Sox2 binds to the active *Ptbp1* promoter in neural progenitor cells.